Published for SISSA by Springer

Received: July 28, 2023
Accepted: August 22, 2023
Published: August 30, 2023

Axial-vector transition form factors and $e^+e^- \to f_1\pi^+\pi^-$

JHEP08(2023)209

Martin Hoferichter,[a] **Bastian Kubis**[b] **and Marvin Zanke**[b]

[a] *Albert Einstein Center for Fundamental Physics, Institute for Theoretical Physics, University of Bern, Sidlerstrasse 5, 3012 Bern, Switzerland*

[b] *Helmholtz-Institut für Strahlen- und Kernphysik (Theorie) and Bethe Center for Theoretical Physics, Universität Bonn, 53115 Bonn, Germany*

E-mail: hoferichter@itp.unibe.ch, kubis@hiskp.uni-bonn.de, zanke@hiskp.uni-bonn.de

Abstract: We study the transition form factors (TFFs) of axial-vector mesons in the context of currently available experimental data, including new constraints from $e^+e^- \to f_1(1285)\pi^+\pi^-$ that imply stringent limits on the high-energy behavior and, for the first time, allow us to provide an unambiguous determination of the couplings corresponding to the two antisymmetric TFFs. We discuss how these constraints can be implemented in a vector-meson-dominance picture, and, in combination with contributions from the light-cone expansion, construct TFFs as input for the evaluation of axial-vector contributions to hadronic light-by-light scattering in the anomalous magnetic moment of the muon.

Keywords: Chiral Lagrangian, Precision QED

ArXiv ePrint: 2307.14413

https://doi.org/10.1007/JHEP08(2023)209

Contents

1 Introduction **1**

2 Axial-vector transition form factors **3**

3 Vector-meson dominance **5**
3.1 Isovector contributions 5
3.2 Isoscalar contributions 7

4 Observables **7**
4.1 $e^+e^- \to e^+e^- f_1$ 7
4.2 $f_1 \to \rho\gamma$ and $f_1 \to \phi\gamma$ 8
4.3 $f_1 \to e^+e^-$ 9
4.4 $e^+e^- \to f_1\rho$ 10
4.5 $e^+e^- \to f_1\pi^+\pi^-$ 13

5 Phenomenological analysis **14**
5.1 Data input for $e^+e^- \to e^+e^- f_1$ and $f_1 \to V\gamma$ 14
5.2 Data input for $e^+e^- \to f_1\pi^+\pi^-$ 14
5.3 Global fit 16
5.4 Final representations 18

6 Conclusions **19**

A Constants and parameters **20**

1 Introduction

The transition form factors (TFFs) of axial-vector mesons are crucial for estimating the hadronic light-by-light (HLbL) contribution to the anomalous magnetic moment of the muon a_μ, in particular, for intermediate photon virtualities and the transition to short-distance constraints (SDCs). At present, the axial-vector contribution included in the Standard-Model prediction for a_μ [1–28] is responsible for a large fraction of the final uncertainty, $a_\mu^{\text{HLbL}} = 92(19) \times 10^{-11}$ [1, 14, 18–26, 29–34], especially, when taking into account the interplay with SDCs. In view of the expected experimental improvements beyond the current world average [35–39], the uncertainty in the HLbL contribution should be reduced by another factor of 2 to ensure that it does not play a role in the interpretation of the experiment [40, 41]. Such improvements are ongoing, both in lattice QCD [42–46] and with data-driven methods, including the derivation of higher-order SDCs [47–49], their implementation [50–56], and dispersion relations [57–60]. In particular, to evaluate the axial-vector contributions, one needs robust input for their TFFs. To this end, constraints on the asymptotic behavior have been derived from the light-cone expansion (LCE) [61] and available data evaluated in a vector-meson-dominance (VMD) inspired parameterization [62], but, due to scarcity of data, no sufficiently complete and reliable solutions have been obtained so far, with ambiguities mostly affecting the determination of the two antisymmetric TFFs.

This is in large part because the interaction of an axial-vector resonance A with two electromagnetic currents is suppressed by the LANDAU–YANG theorem [63, 64] — stating that a spin-1 particle cannot decay into two on-shell photons — so that all observables require at least one non-zero virtuality. Some data are available for the space-like process $e^+e^- \to e^+e^-A$, for $A = f_1 \equiv f_1(1285)$ and $A = f_1' \equiv f_1(1420)$ [65–70], allowing one to extract the equivalent two-photon decay widths $\tilde{\Gamma}_{\gamma\gamma}$ and, thereby, the mixing angle between the two f_1 states. Accordingly, if $U(3)$ symmetry is assumed, it suffices to determine the TFFs for the $f_1(1285)$ to be able to estimate the effect of the entire triplet including the $a_1(1260)$. Focusing, therefore, on the f_1 resonance, for which most data are available, we compiled the constraints that follow from the radiative decays $f_1 \to \rho\gamma$ and $f_1 \to \phi\gamma$, as well as $f_1 \to 4\pi$ and $f_1 \to e^+e^-$ in ref. [62], improving on previous work [71, 72] by employing parameterizations that ensure the absence of kinematic singularities, include SDCs, and incorporate the spectral functions of the isovector resonances. We found that, unfortunately, the decay $f_1 \to 4\pi$ does not provide any meaningful input for the TFFs, since dominated by $f_1 \to a_1\pi \to \rho\pi\pi \to 4\pi$, while $f_1 \to e^+e^-$ would, in principle, be a very interesting observable, yet not at the current level of precision [73].

Ultimately, the currently available data were not sufficient to identify a unique solution for all three TFFs, especially the normalizations of the two antisymmetric TFFs and the momentum dependence of all three TFFs were only poorly determined. In the future, these limitations could be overcome by better data for $e^+e^- \to e^+e^-f_1$ and $f_1 \to e^+e^-$; in this paper, we instead propose to study existing data for $e^+e^- \to f_1\pi^+\pi^-$ [74, 75].[1] This process is also sensitive to all three TFFs, for one photon virtuality centered at the ρ mass and the other one determined by the center-of-mass energy of the e^+e^- pair. Phenomenologically, the reaction displays prominent resonance features from excited ρ resonances [88], primarily the $\rho(2150)$, but, when interpreted as a limit on the non-resonant contribution, entails powerful constraints on the TFFs of the f_1, both on the asymptotic behavior and the respective normalizations.

The outline of the paper is as follows: we first review the basic formalism for the axial-vector TFFs in section 2, and then define improved VMD parameterizations in section 3 that implement the asymptotic behavior observed in $e^+e^- \to f_1\pi^+\pi^-$. In section 4, we summarize the previous observables and present the formalism in which we will analyze

[1]The measurement of the $e^+e^- \to 2(\pi^+\pi^-)\eta$ [74] and $e^+e^- \to K_S K^\pm \pi^\mp \pi^+\pi^-$ [75] cross sections, in which the f_1 peak can be identified, is partly motivated by hadronic vacuum polarization (HVP). The impact of such high-multiplicity channels on the HVP contribution to a_μ, though, is much smaller than the current tensions observed between data-driven evaluations [6–12, 76–80] and lattice QCD [81–85], e.g., $a_\mu^{\text{HVP}}[2(\pi^+\pi^-)\eta] = 0.8(1) \times 10^{-11}$ [11] is at the same level as potential uncertainties from $\mathcal{O}(\alpha^4)$ hadronic corrections [86]. The CMD-3 measurement of $e^+e^- \to 3(\pi^+\pi^-)\pi^0$ [87] includes results for $e^+e^- \to 2(\pi^+\pi^-)\eta$, but no additional information on $e^+e^- \to f_1\pi^+\pi^-$.

JHEP08(2023)209

$e^+e^- \to f_1\pi^+\pi^-$. The phenomenological analysis, including a review of the data base, a global fit, and a summary of the resulting TFF parameterizations, will be presented in section 5, before concluding in section 6. Finally, in appendix A, we collect constants and parameters used throughout this work.

2 Axial-vector transition form factors

The helicity amplitudes for the decay of an axial-vector meson into two virtual photons, $A(P,\lambda_A) \to \gamma^*(q_1,\lambda_1)\gamma^*(q_2,\lambda_2)$, are given by [61, 62]

$$\mathcal{M}\big(\{A,\lambda_A\} \to \{\gamma^*,\lambda_1\}\{\gamma^*,\lambda_2\}\big) = e^2\epsilon_\mu^{\lambda_1\,*}(q_1)\epsilon_\nu^{\lambda_2\,*}(q_2)\epsilon_\alpha^{\lambda_A}(P)\mathcal{M}^{\mu\nu\alpha}(q_1,q_2), \tag{2.1}$$

where, following the Bardeen–Tung–Tarrach procedure [89, 90], the tensor matrix element $\mathcal{M}^{\mu\nu\alpha}(q_1,q_2)$ can be decomposed into three independent Lorentz structures and form factors $\mathcal{F}_i(q_1^2,q_2^2)$ that are free of kinematic singularities according to

$$\mathcal{M}^{\mu\nu\alpha}(q_1,q_2) = \frac{i}{m_A^2}\sum_{i=\mathrm{a}_1,\mathrm{a}_2,\mathrm{s}} T_i^{\mu\nu\alpha}(q_1,q_2)\mathcal{F}_i(q_1^2,q_2^2). \tag{2.2}$$

Here, m_A is the mass of the respective axial-vector meson and the structures

$$\begin{aligned}
T_{\mathrm{a}_1}^{\mu\nu\alpha}(q_1,q_2) &= \epsilon^{\mu\nu\beta\gamma}q_{1\beta}q_{2\gamma}(q_1^\alpha - q_2^\alpha),\\
T_{\mathrm{a}_2}^{\mu\nu\alpha}(q_1,q_2) &= \frac{1}{2}q_{1\beta}q_{2\gamma}\left(\epsilon^{\alpha\nu\beta\gamma}q_1^\mu + \epsilon^{\alpha\mu\beta\gamma}q_2^\nu\right) + \frac{1}{2}\epsilon^{\alpha\mu\nu\beta}(q_{2\beta}q_1^2 + q_{1\beta}q_2^2),\\
T_{\mathrm{s}}^{\mu\nu\alpha}(q_1,q_2) &= \frac{1}{2}q_{1\beta}q_{2\gamma}\left(\epsilon^{\alpha\nu\beta\gamma}q_1^\mu - \epsilon^{\alpha\mu\beta\gamma}q_2^\nu\right) + \frac{1}{2}\epsilon^{\alpha\mu\nu\beta}(q_{2\beta}q_1^2 - q_{1\beta}q_2^2)
\end{aligned} \tag{2.3}$$

are completely antisymmetric (a) or symmetric (s) under photon crossing ($\mu \leftrightarrow \nu$ and $q_1 \leftrightarrow q_2$); similarly, the associated form factors obey the indicated symmetry properties under the exchange of momenta, $q_1^2 \leftrightarrow q_2^2$. Furthermore, the prefactor i/m_A^2 in eq. (2.2) is chosen to obtain dimensionless TFFs with real-valued normalization and the Levi-Civita tensor is used in the convention $\epsilon^{0123} = +1$. For the formulation of SDCs and the analysis of the L3 data for $e^+e^- \to e^+e^- f_1$, see section 4.1, it is also useful to consider the basis defined by

$$\begin{aligned}
\mathcal{F}_1(q_1^2,q_2^2) &= \mathcal{F}_{\mathrm{a}_1}(q_1^2,q_2^2),\\
\mathcal{F}_2(q_1^2,q_2^2) &= \frac{1}{2}\big[\mathcal{F}_{\mathrm{a}_2}(q_1^2,q_2^2) + \mathcal{F}_{\mathrm{s}}(q_1^2,q_2^2)\big],\\
\mathcal{F}_3(q_1^2,q_2^2) &= \frac{1}{2}\big[\mathcal{F}_{\mathrm{a}_2}(q_1^2,q_2^2) - \mathcal{F}_{\mathrm{s}}(q_1^2,q_2^2)\big].
\end{aligned} \tag{2.4}$$

Since the Landau–Yang theorem [63, 64] forbids the decay into two on-shell photons, one commonly defines the so-called equivalent two-photon decay width as [67]

$$\tilde{\Gamma}_{\gamma\gamma} = \lim_{q_1^2\to 0}\frac{1}{2}\frac{m_A^2}{q_1^2}\Gamma(A \to \gamma_{\mathrm{L}}^*\gamma_{\mathrm{T}}), \tag{2.5}$$

with one longitudinal quasi-real photon γ_{L}^*, the spin-averaged — longitudinal-transversal (LT) — width

$$\Gamma(A \to \gamma_{\mathrm{L}}^* \gamma_{\mathrm{T}}) = \frac{1}{3} \sum_{\substack{\lambda_A=\{0,\pm\} \\ \lambda_2=\pm}} \int \mathrm{d}\Gamma^{0\lambda_2|\lambda_A}_{A\to\gamma^*\gamma^*}\Big|_{q_2^2=0}, \tag{2.6}$$

and the differential decay width for fixed polarization

$$\mathrm{d}\Gamma^{\lambda_1\lambda_2|\lambda_A}_{A\to\gamma^*\gamma^*} = \frac{1}{32\pi^2 m_A^2} \frac{\sqrt{\lambda(m_A^2, q_1^2, q_2^2)}}{2m_A} |\mathcal{M}(\{A,\lambda_A\} \to \{\gamma^*,\lambda_1\}\{\gamma^*,\lambda_2\})|^2 \mathrm{d}\Omega, \tag{2.7}$$

where Ω is the center-of-mass solid angle and $\lambda(a,b,c) = a^2 + b^2 + c^2 - 2ab - 2ac - 2bc$ is the Källén function. In terms of the above form factors, one finds

$$\tilde{\Gamma}_{\gamma\gamma} = \frac{\pi\alpha^2}{48} m_A |\mathcal{F}_{\mathrm{s}}(0,0)|^2, \tag{2.8}$$

where $\alpha = e^2/(4\pi)$ is the fine-structure constant.

The asymptotic behavior of the axial-vector TFFs can be analyzed by means of the LCE, leading to [61]

$$\begin{aligned}
\mathcal{F}_{\mathrm{a}_1}(q_1^2, q_2^2) &= \mathcal{O}(1/Q^6), \\
\mathcal{F}_{\mathrm{a}_2}(q_1^2, q_2^2) &= \frac{F^{\mathrm{eff}}_{f_1} m^3_{f_1}}{Q^4} f_{\mathrm{a}_2}(w) + \mathcal{O}(1/Q^6), \qquad f_{\mathrm{a}_2}(w) = \frac{3}{4w^3}\left(6 + \frac{3-w^2}{w}\log\frac{1-w}{1+w}\right), \\
\mathcal{F}_{\mathrm{s}}(q_1^2, q_2^2) &= \frac{F^{\mathrm{eff}}_{f_1} m^3_{f_1}}{Q^4} f_{\mathrm{s}}(w) + \mathcal{O}(1/Q^6), \qquad f_{\mathrm{s}}(w) = -\frac{3}{2w^3}\left(2w + \log\frac{1-w}{1+w}\right),
\end{aligned} \tag{2.9}$$

where

$$Q^2 = \frac{q_1^2 + q_2^2}{2} \in [0,\infty), \qquad w = \frac{q_1^2 - q_2^2}{q_1^2 + q_2^2} \in [-1,1] \tag{2.10}$$

denote the average photon virtuality and asymmetry parameter, respectively. In the above, we furthermore introduced the effective decay constant

$$F_A^{\mathrm{eff}} = 4\sum_a C_a F_A^a, \tag{2.11}$$

with the decay constants F_A^a defined via

$$\langle 0|\bar{q}(0)\gamma_\mu\gamma_5 \frac{\lambda^a}{2} q(0)|A(P,\lambda_A)\rangle = F_A^a m_A \epsilon_\mu. \tag{2.12}$$

The Gell-Mann matrices λ_a and the conveniently normalized unit matrix $\lambda_0 = \sqrt{2/3}\,\mathbb{1}$ determine the flavor decomposition, with the flavor weights C_a in the effective decay constant given by $C_0 = 2/(3\sqrt{6})$, $C_3 = 1/6$, and $C_8 = 1/(6\sqrt{3})$. In the symmetric doubly-virtual direction, the $\mathcal{O}(1/q^4)$ limits become ($\lambda \approx 1$) [62]

$$\begin{aligned}
\mathcal{F}_{\mathrm{a}_2}(q^2, \lambda q^2) &= -\frac{6F^{\mathrm{eff}}_{f_1} m^3_{f_1}}{q^4} k(\lambda) + \mathcal{O}(1/q^6), \qquad \mathcal{F}_{\mathrm{s}}(q^2, q^2) = \frac{F^{\mathrm{eff}}_{f_1} m^3_{f_1}}{q^4} + \mathcal{O}(1/q^6), \\
k(\lambda) &= \frac{3\lambda^2 - (\lambda^2 + 4\lambda + 1)\log\lambda - 3}{(\lambda-1)^4} = \mathcal{O}(\lambda - 1),
\end{aligned} \tag{2.13}$$

but all singly-virtual limits of $\mathcal{F}_{\mathrm{a}_2/\mathrm{s}}(q_1^2,q_2^2)$ diverge in the symmetrized basis. However, physical helicity amplitudes depend on linear combinations of the TFFs in such a way that only well-defined limits contribute to observables [61, 62], which implies that $\mathcal{F}_2(q^2,0)$ and $\mathcal{F}_3(0,q^2)$ have finite limits, while the opposite cases diverge.

3 Vector-meson dominance

The parameterization of the TFFs inspired by VMD is based on their decomposition into isovector and isoscalar components. Using $U(3)$ symmetry, one can deduce the ratio [62]

$$R_{\mathrm{S/V}} = \frac{\sqrt{2}-\tan\theta_A}{3\left(\sqrt{2}+\tan\theta_A\right)} = -4.7(3.4)\% \tag{3.1}$$

of isoscalar to isovector contributions for the $f_1\gamma^*\gamma^*$ coupling, where we inserted the L3 mixing angle $\theta_A = 62(5)^\circ$ [69, 70],[2] derived from

$$\frac{\tilde{\Gamma}^{f_1}_{\gamma\gamma}}{\tilde{\Gamma}^{f_1'}_{\gamma\gamma}} = \frac{m_{f_1}}{m_{f_1'}}\cot^2(\theta_A-\theta_0), \qquad \theta_0 = \arcsin\frac{1}{3}, \tag{3.2}$$

for the corresponding $J^{PC}=1^{++}$ axial-vector nonet with the mixing pattern

$$\begin{pmatrix} f_1 \\ f_1' \end{pmatrix} = \begin{pmatrix} \cos\theta_A & \sin\theta_A \\ -\sin\theta_A & \cos\theta_A \end{pmatrix}\begin{pmatrix} f^0 \\ f^8 \end{pmatrix}. \tag{3.3}$$

Hence, it is the isovector channel that dominates the process, with small isoscalar corrections at the level of 5%.

The minimal particle content necessary for a VMD construction of TFFs that individually obey the asymptotic constraints summarized in section 2 requires the inclusion of three multiplets. More specifically, we will use $\rho\equiv\rho(770)$, $\rho'\equiv\rho(1450)$, and $\rho''\equiv\rho(1700)$ for the isovector contributions and $\omega\equiv\omega(782)$, $\omega'\equiv\omega(1420)$, $\omega''\equiv\omega(1650)$ as well as $\phi\equiv\phi(1020)$, $\phi'\equiv\phi(1680)$, $\phi''\equiv\phi(2170)$ for the isoscalar contributions. The introduction of a third multiplet, as required to obtain the correct asymptotic behavior for the antisymmetric TFFs, goes beyond the parameterizations of ref. [62], ultimately, because the data on $e^+e^-\to f_1\pi^+\pi^-$ demand such a steep decrease, including in kinematic configurations in which one virtuality is kept fixed at a finite but non-zero value.

3.1 Isovector contributions

In the space-like region, $q_i^2<0$, we propose to extend the isovector parameterizations from ref. [62] as follows:

$$\begin{aligned}\mathcal{F}^{I=1}_{\mathrm{a}_{1/2}}(q_1^2,q_2^2) = C_{\mathrm{a}_{1/2}}\Bigg[&\frac{(1-\epsilon^{(1)}_{\mathrm{a}_{1/2}}-\epsilon^{(2)}_{\mathrm{a}_{1/2}})M_\rho^2 M_{\rho'}^2}{(q_1^2-M_\rho^2)(q_2^2-M_{\rho'}^2)} + \frac{\epsilon^{(1)}_{\mathrm{a}_{1/2}}M_\rho^2 M_{\rho''}^2}{(q_1^2-M_\rho^2)(q_2^2-M_{\rho''}^2)}\\ &+\frac{\epsilon^{(2)}_{\mathrm{a}_{1/2}}M_{\rho'}^2 M_{\rho''}^2}{(q_1^2-M_{\rho'}^2)(q_2^2-M_{\rho''}^2)}\Bigg] - (q_1\leftrightarrow q_2),\end{aligned}$$

[2] This determination of θ_A assumes $B(f_1'\to K\bar{K}\pi)=1$, supported by $\Gamma(f_1'\to\eta\pi\pi)/\Gamma(f_1'\to K\bar{K}\pi)<0.1$ [91] and $\Gamma(f_1'\to a_0(980)\pi)/\Gamma(f_1'\to K\bar{K}\pi)=0.040(14)$ [92].

$$\mathcal{F}_{\mathrm{s}}^{I=1}(q_1^2,q_2^2) = C_{\mathrm{s}}\Bigg[\frac{(1-\epsilon_{\mathrm{s}}^{(1)}-\epsilon_{\mathrm{s}}^{(2)})M_\rho^4}{(q_1^2-M_\rho^2)(q_2^2-M_\rho^2)}+\frac{(\epsilon_{\mathrm{s}}^{(1)}/2)M_\rho^2M_{\rho'}^2}{(q_1^2-M_\rho^2)(q_2^2-M_{\rho'}^2)} \\ +\frac{(\epsilon_{\mathrm{s}}^{(1)}/2)M_{\rho'}^2M_\rho^2}{(q_1^2-M_{\rho'}^2)(q_2^2-M_\rho^2)}+\frac{\epsilon_{\mathrm{s}}^{(2)}M_{\rho'}^4}{(q_1^2-M_{\rho'}^2)(q_2^2-M_{\rho'}^2)}\Bigg], \tag{3.4}$$

first given in this form to emphasize that, upon a partial-fraction decomposition, each term corresponds to adding vector-meson propagators with fixed coefficients. To implement the correct singly-virtual asymptotic behavior, we choose

$$\epsilon_{\mathrm{a}_{1/2}}^{(1)} = -\frac{M_{\rho'}^2}{M_{\rho''}^2-M_{\rho'}^2+M_\rho^2}, \qquad \epsilon_{\mathrm{a}_{1/2}}^{(2)} = \frac{M_\rho^2}{M_{\rho''}^2-M_{\rho'}^2+M_\rho^2},$$
$$\epsilon_{\mathrm{s}}^{(1)} = -\frac{2M_\rho^2M_{\rho'}^2}{(M_{\rho'}^2-M_\rho^2)^2}, \qquad \epsilon_{\mathrm{s}}^{(2)} = \frac{M_\rho^4}{(M_{\rho'}^2-M_\rho^2)^2}, \tag{3.5}$$

leading to

$$\mathcal{F}_{\mathrm{a}_{1/2}}^{I=1}(q_1^2,q_2^2) = \frac{C_{\mathrm{a}_{1/2}}\zeta_\rho M_\rho^4M_{\rho'}^4M_{\rho''}^4(q_1^2-q_2^2)}{(q_1^2-M_\rho^2)(q_2^2-M_\rho^2)(q_1^2-M_{\rho'}^2)(q_2^2-M_{\rho'}^2)(q_1^2-M_{\rho''}^2)(q_2^2-M_{\rho''}^2)},$$
$$\mathcal{F}_{\mathrm{s}}^{I=1}(q_1^2,q_2^2) = \frac{C_{\mathrm{s}}M_\rho^4M_{\rho'}^4}{(q_1^2-M_\rho^2)(q_2^2-M_\rho^2)(q_1^2-M_{\rho'}^2)(q_2^2-M_{\rho'}^2)}, \tag{3.6}$$

with

$$\zeta_V = \frac{(M_{V''}^2-M_{V'}^2)(M_{V''}^2-M_V^2)(M_{V'}^2-M_V^2)}{M_{V''}^2M_{V'}^2M_V^2(M_{V''}^2-M_{V'}^2+M_V^2)}. \tag{3.7}$$

The resulting asymptotic behavior of the TFFs becomes

$$\mathcal{F}_{\mathrm{a}_{1/2}}^{I=1}(q_1^2,q_2^2) \propto \frac{1}{q_2^4}, \qquad \mathcal{F}_{\mathrm{a}_{1/2}}^{I=1}(q^2,\lambda q^2) \propto \frac{1-\lambda}{\lambda^3}\frac{1}{q^{10}},$$
$$\mathcal{F}_{\mathrm{s}}^{I=1}(q_1^2,q_2^2) \propto \frac{1}{q_2^4}, \qquad \mathcal{F}_{\mathrm{s}}^{I=1}(q^2,\lambda q^2) \propto \frac{1}{q^8}, \tag{3.8}$$

with q_1^2 fixed to a finite value distinct from q_2^2 (left) and in the doubly-virtual direction (right). Crucially, the singly-virtual asymptotics now match the LCE result from section 2 for arbitrary fixed q_1^2, which, for $q_1^2 = M_\rho^2$, is mandatory for a realistic description of the $e^+e^- \to f_1\pi^+\pi^-$ data (the opposite case with fixed q_2^2 follows from symmetry).[3] For time-like applications, the replacements $M^2 \to M^2 - iM\Gamma$ apply in the denominators of eq. (3.6), i.e., after imposing the asymptotic behavior of the TFFs; due to the large widths of the ρ-like mesons, a narrow-width approximation, $M^2 \to M^2 - i\epsilon$ in the denominators, in

[3]For $\mathcal{F}_{\mathrm{a}_1}^{I=1}(q_1^2,q_2^2)$, the LCE predicts an even faster decrease in the singly-virtual direction, but we do not consider yet another multiplet for the following reasons: (i) information from the LCE on this TFF is limited, i.e., no non-vanishing contribution survives at $\mathcal{O}(1/Q^4)$, in such a way that, in contrast to the other TFFs, we cannot add an LCE term to repair the behavior in the doubly-virtual direction and thus need to choose a compromise; (ii) the fit to $e^+e^- \to f_1\pi^+\pi^-$ produces a small coupling C_{a_1}, in line with the LCE suppression; (iii) another multiplet would have a mass already in the energy range in which the data are to be described, so that no meaningful suppression could be generated even when introducing another state.

general becomes insufficient here. A consequence of the faster decrease in the singly-virtual directions concerns an even faster decrease in the doubly-virtual case, much below the LCE expectation. Accordingly, in the final representation for the TFFs, we add the asymptotic contribution [62]

$$
\begin{aligned}
\mathcal{F}_{\mathrm{a}_2}^{\mathrm{asym}}(q_1^2,q_2^2) &= 3F_{f_1}^{\mathrm{eff}}m_{f_1}^3\left(q_1^2-q_2^2\right)\int_{s_\mathrm{m}}^{\infty}\mathrm{d}x\,\frac{q_1^2q_2^2-x^2+x(q_1^2+q_2^2)}{(x-q_1^2)^3(x-q_2^2)^3},\\
\mathcal{F}_{\mathrm{s}}^{\mathrm{asym}}(q_1^2,q_2^2) &= 3F_{f_1}^{\mathrm{eff}}m_{f_1}^3\int_{s_\mathrm{m}}^{\infty}\mathrm{d}x\,\frac{(q_1^2+q_2^2)(x^2-q_1^2q_2^2)-x(q_1^2-q_2^2)^2}{(x-q_1^2)^3(x-q_2^2)^3},
\end{aligned}
\tag{3.9}
$$

where s_m is a parameter that determines the scale of the transition. The implementation of these asymptotic contributions, or their variant including mass effects [62], becomes relevant for the axial-vector contributions in the HLbL loop integral. Here, we focus on the determination of the low-energy couplings in the VMD component of the parameterization, as can be obtained from $e^+e^-\to f_1\pi^+\pi^-$.

3.2 Isoscalar contributions

In complete analogy to the above, the isoscalar parts of the form factors are parameterized according to[4]

$$
\begin{aligned}
\mathcal{F}_{\mathrm{a}_{1/2}}^{I=0}(q_1^2,q_2^2) &= \sum_{V=\omega,\phi}\frac{C_{\mathrm{a}_{1/2}}^{V}\zeta_V M_V^4M_{V'}^4M_{V''}^4(q_1^2-q_2^2)}{(q_1^2-M_V^2)(q_2^2-M_V^2)(q_1^2-M_{V'}^2)(q_2^2-M_{V'}^2)(q_1^2-M_{V''}^2)(q_2^2-M_{V''}^2)},\\
\mathcal{F}_{\mathrm{s}}^{I=0}(q_1^2,q_2^2) &= \sum_{V=\omega,\phi}\frac{C_{\mathrm{s}}^{V}M_V^4M_{V'}^4}{(q_1^2-M_V^2)(q_2^2-M_V^2)(q_1^2-M_{V'}^2)(q_2^2-M_{V'}^2)},
\end{aligned}
\tag{3.10}
$$

with the same asymptotic properties as in eq. (3.8). Again, time-like applications imply the replacements $M^2\to M^2-iM\Gamma$ in the denominators, since the large widths of the excited isoscalar resonances do not allow for a narrow-width approximation. Finally, under the assumption of $U(3)$ symmetry, the isoscalar coupling constants can be related to the isovector analogs, leading to the approximations [62]

$$
\begin{aligned}
R^{\omega} &= \frac{C_{\mathrm{a}_{1/2}}^{\omega}}{C_{\mathrm{a}_{1/2}}}=\frac{C_{\mathrm{s}}^{\omega}}{C_{\mathrm{s}}}=\frac{1}{9},\\
R^{\phi} &= \frac{C_{\mathrm{a}_{1/2}}^{\phi}}{C_{\mathrm{a}_{1/2}}}=\frac{C_{\mathrm{s}}^{\phi}}{C_{\mathrm{s}}}=\frac{2\sqrt{2}}{9}\cot(\theta_A+\theta_1)=-0.158(34),
\end{aligned}
\tag{3.11}
$$

with $\theta_1=\arctan\sqrt{2}=(\pi+2\theta_0)/4$.

4 Observables

4.1 $e^+e^-\to e^+e^-f_1$

The equivalent two-photon decay width $\tilde{\Gamma}_{\gamma\gamma}^{f_1}=3.5(6)(5)\,\mathrm{keV}$, as measured by the L3 collaboration [69], determines the normalization of the symmetric TFF, see eq. (2.8). Taking

[4]We assume ideal mixing for the vector mesons, which prevents crossed terms involving ω and ϕ states.

into account the isoscalar contributions, $|\mathcal{F}_{\mathrm{s}}^{I=1}(0,0)+\mathcal{F}_{\mathrm{s}}^{I=0}(0,0)| = (1+R^\omega+R^\phi)|C_{\mathrm{s}}| = 0.953(34)|C_{\mathrm{s}}|$, we have

$$C_{\mathrm{s}} = 0.93(11), \tag{4.1}$$

where we followed the sign convention of ref. [62].

The singly-virtual VMD limits can be further constrained by matching the L3 parameterization onto the full description of the $e^+e^- \to e^+e^- f_1$ cross section [61],

$$\left|\left(1-\frac{q^2}{m_{f_1}^2}\right)\mathcal{F}_1(q^2,0) - \frac{q^2}{m_{f_1}^2}\mathcal{F}_2(q^2,0)\right|^2 - \frac{2q^2}{m_{f_1}^2}|\mathcal{F}_2(q^2,0)|^2 = \frac{-q^2}{m_{f_1}^2}\left(2-\frac{q^2}{m_{f_1}^2}\right)|\mathcal{F}_{\mathrm{D}}(q^2,0)|^2, \tag{4.2}$$

where

$$\mathcal{F}_{\mathrm{D}}(q^2,0) = \frac{\mathcal{F}_{\mathrm{D}}(0,0)}{(1-q^2/\Lambda_{\mathrm{D}}^2)^2} \tag{4.3}$$

is the dipole ansatz assumed in ref. [69] and the form factors are given in the basis of eq. (2.4). While the normalization agrees by construction, matching the slopes at $q^2=0$ leads to

$$\begin{aligned}\frac{2}{\Lambda_{\mathrm{D}}^2} = \frac{1}{N_{\omega\phi}}\Bigg[&\frac{1}{M_\rho^2}+\frac{1}{M_{\rho'}^2} + R^\omega\left(\frac{1}{M_\omega^2}+\frac{1}{M_{\omega'}^2}\right) + R^\phi\left(\frac{1}{M_\phi^2}+\frac{1}{M_{\phi'}^2}\right) \\ &+ (\zeta_\rho+\zeta_\omega R^\omega+\zeta_\phi R^\phi)\frac{C_{\mathrm{a}_1}+C_{\mathrm{a}_2}}{C_{\mathrm{s}}} - \frac{m_{f_1}^2(\zeta_\rho+\zeta_\omega R^\omega+\zeta_\phi R^\phi)^2}{N_{\omega\phi}}\left(\frac{C_{\mathrm{a}_1}}{C_{\mathrm{s}}}\right)^2\Bigg],\end{aligned} \tag{4.4}$$

where the factor $N_{\omega\phi} = 1+R^\omega+R^\phi$ accounts for the isoscalar terms in the normalization.

4.2 $f_1 \to \rho\gamma$ and $f_1 \to \phi\gamma$

From the procedure outlined in ref. [62], it is straightforward to obtain the branching ratio of $f_1 \to V\gamma$, $V=\rho,\omega,\phi$, in the form

$$B(f_1\to V\gamma) = (R^V)^2\frac{B_1^V\big(\tilde{C}_{\mathrm{a}_1}^V\big)^2 + B_2^V\big(\tilde{C}_{\mathrm{a}_2}^V+\tilde{C}_{\mathrm{s}}^V\big)^2 - B_3^V\tilde{C}_{\mathrm{a}_1}^V\big(\tilde{C}_{\mathrm{a}_2}^V+\tilde{C}_{\mathrm{s}}^V\big)}{\Gamma_f}, \tag{4.5}$$

where we defined

$$\begin{aligned} B_1^V &= \frac{\alpha|g_{V\gamma}|^2\big(m_{f_1}^2-M_V^2\big)^5}{24m_{f_1}^9}, \qquad & B_2^V &= \frac{\alpha|g_{V\gamma}|^2M_V^2\big(m_{f_1}^2-M_V^2\big)^3\big(m_{f_1}^2+M_V^2\big)}{96m_{f_1}^9}, \\ B_3^V &= \frac{\alpha|g_{V\gamma}|^2M_V^2\big(m_{f_1}^2-M_V^2\big)^4}{24m_{f_1}^9}, \end{aligned} \tag{4.6}$$

and the couplings

$$\tilde{C}_{\mathrm{a}_{1/2}}^V = J_{\mathrm{a}}^V C_{\mathrm{a}_{1/2}}, \qquad \tilde{C}_{\mathrm{s}}^V = J_{\mathrm{s}}^V C_{\mathrm{s}} \tag{4.7}$$

are rescaled by

$$J_{\mathrm{a}}^V = \frac{M_{V''}^2-M_{V'}^2}{M_{V''}^2-M_{V'}^2+M_V^2}, \qquad J_{\mathrm{s}}^V = \frac{M_{V'}^2}{M_{V'}^2-M_V^2}. \tag{4.8}$$

The normalizations R^V, $V=\omega,\phi$, are given by eq. (3.11), and $R^\rho = 1$.

	Narrow-resonance limit		Spectral function for ρ	
$D_1^{I=1} \times 10^3$	$0.23 - 1.68i$		$0.15 - 1.42i$	
$D_2^{I=1} \times 10^3$	$-1.70 + 1.81i$		$-1.36 + 1.64i$	
$D_3^{I=1} \times 10^3$	$1.25 + 4.38i$		$3.00 + 4.10i$	
$D_1^{\omega} \times 10^3$	$0.30 - 1.65i$			
$D_2^{\omega} \times 10^3$	$-1.89 + 1.81i$			
$D_3^{\omega} \times 10^3$	$1.06 + 4.61i$			
$D_1^{\phi} \times 10^3$	$-0.98 - 1.09i$			
$D_2^{\phi} \times 10^3$	$0.19 + 2.42i$			
$D_3^{\phi} \times 10^3$	$6.02 + 5.97i$			
$D_{\text{asym}} \times 10^3$	0.125(12)	0.032(3)	0.017(2)	0.009(1)

Table 1. Numerical values for the coefficients D_i^I in eq. (4.13) (obtained using the *Cuba* library [93]). The total isoscalar one follows as $D_i^{I=0} = R^{\omega} D_i^{\omega} + R^{\phi} D_i^{\phi}$, and D_{asym} is given for the matching points $\sqrt{s_{\text{m}}} \in \{1.0, 1.3, 1.5, 1.7\}$ GeV. The left column gives the reference point for which the widths of all vector mesons are neglected and the right column the more realistic case that includes the spectral function of the ρ (used as input in table 3).

In addition, for $V = \rho$, information on the helicity amplitudes is available. The spin-averaged amplitude squared of the corresponding process $f_1 \to \rho\gamma \to \pi^+\pi^-\gamma$, with the subsequent decay of an on-shell ρ meson, is of the generic form

$$\left|\mathcal{M}(f_1 \to \rho\gamma \to \pi^+\pi^-\gamma)\right|^2 = \text{M}_{\text{TT}} \sin^2\theta_{\pi^+\gamma} + \text{M}_{\text{LL}} \cos^2\theta_{\pi^+\gamma}, \tag{4.9}$$

where $\theta_{\pi^+\gamma}$ is the angle between the final-state π^+ and the photon. Similarly to the branching ratio of $f_1 \to \rho\gamma$, the ratio of helicity amplitudes for $f_1 \to \rho\gamma \to \pi^+\pi^-\gamma$ results from a straightforward modification of the result presented in ref. [62],

$$r_{\rho\gamma} = \frac{\text{M}_{\text{LL}}}{\text{M}_{\text{TT}}} = \frac{2m_{f_1}^2 M_\rho^2}{\left[M_\rho^2 - 2\left(m_{f_1}^2 - M_\rho^2\right)\tilde{C}_{\text{a}_1}/\left(\tilde{C}_{\text{a}_2} + \tilde{C}_{\text{s}}\right)\right]^2}. \tag{4.10}$$

4.3 $f_1 \to e^+e^-$

We follow ref. [62] and write the decay rate for $f_1 \to e^+e^-$ as

$$\Gamma(f_1 \to e^+e^-) = \frac{64\pi^3\alpha^4 m_{f_1}}{3}|A_1|^2, \tag{4.11}$$

where the scalar amplitude A_1 is implicitly defined by

$$\mathcal{M}(f_1(P) \to e^+(p_2)e^-(p_1)) = e^4\epsilon_\mu(P)\bar{u}^s(p_1)\gamma^\mu\gamma^5 A_1 v^r(p_2) \tag{4.12}$$

and further decomposes into terms proportional to the three VMD couplings (with isoscalar and isovector coefficients D_i^I) and an asymptotic contribution D_{asym},

$$A_1 = \left(D_1^{I=1} + D_1^{I=0}\right)C_{\text{a}_1} + \left(D_2^{I=1} + D_2^{I=0}\right)C_{\text{a}_2} + \left(D_3^{I=1} + D_3^{I=0}\right)C_{\text{s}} + D_{\text{asym}}. \tag{4.13}$$

JHEP08(2023)209

For the case of products of narrow-resonance propagators as in eq. (3.4), with squared masses x and y, the integral representation

$$D_i = \frac{xy}{16\pi^2 m_{f_1}^4}\int_0^1 \mathrm{d}z\, f_i(x,y,z,m_{f_1}) \tag{4.14}$$

applies, with analytic expressions for the functions $f_i(x,y,z,m_{f_1})$ given in ref. [62]. In the same reference, we also provided evaluations of the asymptotic contribution D_{asym} and studied in detail the sensitivity of the integrals to the spectral functions assumed for ρ and ρ' resonances when going beyond a narrow-resonance picture, to avoid unphysical imaginary parts in the loop integrals [94–96]. In the decay region of the f_1, by far the most important correction arises from the width of the ρ. Here, we provide a simple evaluation of $B(f_1 \to e^+e^-)$ for the representations constructed in section 3 that captures this main effect, to ensure that our final solutions do not conflict with the SND measurement [73]. To this end, we replace

$$\begin{aligned}
\mathcal{F}_{\mathrm{a}_{1/2}}^{I=1}(q_1^2,q_2^2) &\to \frac{C_{\mathrm{a}_{1/2}}}{N_{\mathrm{a}_{1/2}}}\frac{M_{\rho'}^2 M_{\rho''}^2(M_{\rho''}^2-M_{\rho'}^2)(q_1^2-q_2^2)}{(q_1^2-M_{\rho'}^2)(q_2^2-M_{\rho'}^2)(q_1^2-M_{\rho''}^2)(q_2^2-M_{\rho''}^2)}\\
&\qquad\times\frac{1}{\pi}\int_{4M_\pi^2}^\infty \mathrm{d}x\,\frac{x(M_{\rho''}^2-x)(M_{\rho'}^2-x)\rho(x)}{(M_{\rho''}^2-M_{\rho'}^2+x)(q_1^2-x)(q_2^2-x)},\\
\mathcal{F}_{\mathrm{s}}^{I=1}(q_1^2,q_2^2) &\to \frac{C_{\mathrm{s}}}{N_{\mathrm{s}}^2}\frac{M_{\rho'}^4}{(q_1^2-M_{\rho'}^2)(q_2^2-M_{\rho'}^2)}\frac{1}{\pi^2}\int_{4M_\pi^2}^\infty \mathrm{d}x\int_{4M_\pi^2}^\infty \mathrm{d}y\,\frac{xy\rho(x)\rho(y)}{(q_1^2-x)(q_2^2-y)}
\end{aligned}\tag{4.15}$$

in eq. (3.6), where the normalizations $N_{\mathrm{a}_{1/2}}$, N_{s} of the spectral function $\rho(x)$ (taken from refs. [62, 97, 98]) are determined by demanding that the meaning of the couplings $C_{\mathrm{a}_{1/2}}$, C_{s} remain unaltered compared to the zero-width limit; numerical results for the coefficients D_i are collected in table 1.[5] Once improved data on $B(f_1 \to e^+e^-)$ become available, more refined analyses can be performed along the lines of refs. [62, 107].

4.4 $e^+e^- \to f_1\rho$

The scattering process $e^+e^- \to f_1\pi^+\pi^-$ probes the f_1 TFFs in the time-like region via $e^+e^- \to \gamma^* \to f_1\rho \to f_1\pi^+\pi^-$, see figure 1. For our analysis, we thus define amputated $f_1 \to \rho\gamma^*$ form factors, which are related to $\gamma^* \to f_1\rho$ via crossing symmetry, according to

$$\begin{aligned}
\bar{\mathcal{F}}_{\mathrm{a}_{1/2}}^{I=1}(q_2^2) &= C_{\mathrm{a}_{1/2}}\left[\frac{(1-\epsilon_{\mathrm{a}_{1/2}}^{(1)}-\epsilon_{\mathrm{a}_{1/2}}^{(2)})M_\rho^2 M_{\rho'}^2}{q_2^2-M_{\rho'}^2}+\frac{\epsilon_{\mathrm{a}_{1/2}}^{(1)}M_\rho^2 M_{\rho''}^2}{q_2^2-M_{\rho''}^2}\right] = -\frac{C_{\mathrm{a}_{1/2}}\bar{\zeta}_{\mathrm{a}}}{(q_2^2-M_{\rho'}^2)(q_2^2-M_{\rho''}^2)}\\
&\to -\frac{C_{\mathrm{a}_{1/2}}\bar{\zeta}_{\mathrm{a}}}{(q_2^2-M_{\rho'}^2+iM_{\rho'}\Gamma_{\rho'})(q_2^2-M_{\rho''}^2+iM_{\rho''}\Gamma_{\rho''})},\\
\bar{\mathcal{F}}_{\mathrm{s}}^{I=1}(q_2^2) &= C_{\mathrm{s}}\left[\frac{(1-\epsilon_{\mathrm{s}}^{(1)}-\epsilon_{\mathrm{s}}^{(2)})M_\rho^4}{q_2^2-M_\rho^2}+\frac{(\epsilon_{\mathrm{s}}^{(1)}/2)M_\rho^2 M_{\rho'}^2}{q_2^2-M_{\rho'}^2}\right] = -\frac{C_{\mathrm{s}}\bar{\zeta}_{\mathrm{s}}}{(q_2^2-M_\rho^2)(q_2^2-M_{\rho'}^2)}\\
&\to -\frac{C_{\mathrm{s}}\bar{\zeta}_{\mathrm{s}}}{(q_2^2-M_\rho^2+iM_\rho\Gamma_\rho)(q_2^2-M_{\rho'}^2+iM_{\rho'}\Gamma_{\rho'})},
\end{aligned}\tag{4.16}$$

[5] Besides the analytic evaluation using the functions $f_i(x,y,z,m_{f_1})$, we performed cross checks by means of a Passarino–Veltman decomposition, obtained with *FeynCalc* [99–101], and the subsequent calculation of the loop integrals with *Collier* [102–106].

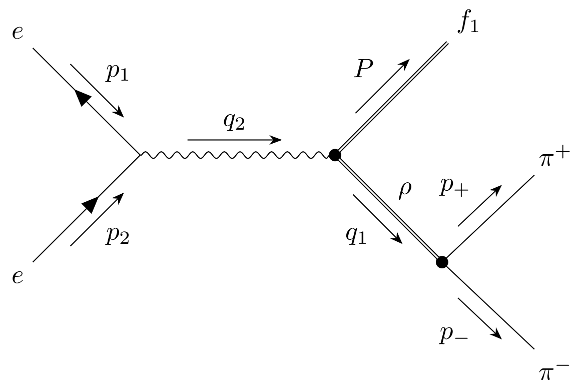

Figure 1. FEYNMAN diagram for $e^+e^- \to f_1\rho \to f_1\pi^+\pi^-$ consistent with $\mathcal{M}(\gamma^* \to f_1\rho^{0*})$.

where

$$\bar{\zeta}_\mathrm{a} = \frac{M_\rho^2 M_{\rho'}^2 M_{\rho''}^2 (M_{\rho''}^2 - M_{\rho'}^2)}{M_{\rho''}^2 - M_{\rho'}^2 + M_\rho^2}, \qquad \bar{\zeta}_\mathrm{s} = \frac{M_\rho^4 M_{\rho'}^4}{M_{\rho'}^2 - M_\rho^2}, \tag{4.17}$$

and a width has been inserted into the denominators for the time-like application.

As a first approximation, we consider the case in which the decay $e^+e^- \to f_1\pi^+\pi^-$ is described by $e^+e^- \to f_1\rho$, see figure 2, whose amplitude can be constructed from eq. (2.2) and eq. (3.4) by amputating the ρ propagator,

$$\begin{aligned} \mathcal{M}(\gamma^* \to f_1\rho^{0*}) = &\frac{e}{\tilde{g}_{\rho\gamma} m_{f_1}^2} \epsilon_\mu^*(q_1)\epsilon_\nu(q_2)\epsilon_\alpha^*(P) \\ &\times \Big[T_{\mathrm{a}_1}^{\mu\nu\alpha}(-q_1,q_2)\bar{\mathcal{F}}_{\mathrm{a}_1}(q_2^2) + T_{\mathrm{a}_2}^{\mu\nu\alpha}(-q_1,q_2)\bar{\mathcal{F}}_{\mathrm{a}_2}(q_2^2) + T_{\mathrm{s}}^{\mu\nu\alpha}(-q_1,q_2)\bar{\mathcal{F}}_{\mathrm{s}}(q_2^2)\Big], \end{aligned} \tag{4.18}$$

and the prefactor follows in analogy to the derivation of $f_1 \to V\gamma$ in ref. [62]. In particular, we have taken over the definition

$$\tilde{g}_{V\gamma} = \frac{M_V^2}{g_{V\gamma}}, \tag{4.19}$$

to establish the connection to $g_{V\gamma}$, which, in a narrow-width approximation, is related to the dilepton decay

$$\Gamma(V \to e^+e^-) = \frac{4\pi\alpha^2}{3|g_{V\gamma}|^2}\left(1 + \frac{2m_e^2}{M_V^2}\right)\sqrt{M_V^2 - 4m_e^2}, \tag{4.20}$$

or, more rigorously, to the residue at the pole [108]. In order to determine the amplitude for $e^+e^- \to \gamma^* \to f_1\rho$, we calculate the diagram shown in figure 2, leading to

$$\begin{aligned} \mathcal{M}(e^+e^- \to f_1\rho) = &\frac{e^2}{\tilde{g}_{\rho\gamma} m_{f_1}^2} \epsilon_\mu^*(q_1)\epsilon_\alpha^*(P)\frac{\bar{v}^s(p_1)\gamma_\nu u^r(p_2)}{q_2^2} \\ &\times \Big[T_{\mathrm{a}_1}^{\mu\nu\alpha}(-q_1,q_2)\bar{\mathcal{F}}_{\mathrm{a}_1}(q_2^2) + T_{\mathrm{a}_2}^{\mu\nu\alpha}(-q_1,q_2)\bar{\mathcal{F}}_{\mathrm{a}_2}(q_2^2) + T_{\mathrm{s}}^{\mu\nu\alpha}(-q_1,q_2)\bar{\mathcal{F}}_{\mathrm{s}}(q_2^2)\Big]\Big|_{q_1^2 = M_\rho^2}, \end{aligned} \tag{4.21}$$

where we dropped an unobservable overall phase.

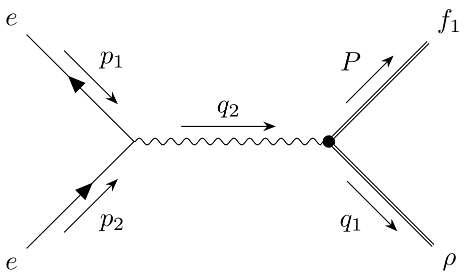

Figure 2. FEYNMAN diagram for $e^+e^- \to f_1\rho$ consistent with $\mathcal{M}(\gamma^* \to f_1\rho^{0*})$.

JHEP08(2023)209

Spin-averaging the squared amplitude and performing the angular integration, we find

$$\begin{aligned}\sigma(e^+e^- \to f_1\rho)(s) = &\frac{e^4|g_{\rho\gamma}|^2|\boldsymbol{p}_\rho|(s+2m_e^2)}{384\pi m_{f_1}^6 M_\rho^4 s^3|\boldsymbol{p}_e|} \\ &\times \Big[T_{\mathrm{a}_1,\mathrm{a}_1}(q_1^2,s)\big|\bar{\mathcal{F}}_{\mathrm{a}_1}(s)\big|^2 + T_{\mathrm{a}_2,\mathrm{a}_2}(q_1^2,s)\big|\bar{\mathcal{F}}_{\mathrm{a}_2}(s)\big|^2 + T_{\mathrm{s},\mathrm{s}}(q_1^2,s)\big|\bar{\mathcal{F}}_{\mathrm{s}}(s)\big|^2 \\ &+ 2T_{\mathrm{a}_1,\mathrm{a}_2}(q_1^2,s)\mathrm{Re}\big[\bar{\mathcal{F}}_{\mathrm{a}_1}(s)\bar{\mathcal{F}}^*_{\mathrm{a}_2}(s)\big] + 2T_{\mathrm{a}_1,\mathrm{s}}(q_1^2,s)\mathrm{Re}\big[\bar{\mathcal{F}}_{\mathrm{a}_1}(s)\bar{\mathcal{F}}^*_{\mathrm{s}}(s)\big] \\ &+ 2T_{\mathrm{a}_2,\mathrm{s}}(q_1^2,s)\mathrm{Re}\big[\bar{\mathcal{F}}_{\mathrm{a}_2}(s)\bar{\mathcal{F}}^*_{\mathrm{s}}(s)\big]\Big]\Big|_{q_1^2=M_\rho^2} \end{aligned} \tag{4.22}$$

for the total cross section, with $s = q_2^2$, initial- and final-state momenta

$$|\boldsymbol{p}_e| = \frac{\sqrt{s-4m_e^2}}{2}, \qquad |\boldsymbol{p}_\rho| = \frac{\sqrt{\lambda(s,q_1^2,m_{f_1}^2)}}{2\sqrt{s}}, \tag{4.23}$$

and the kinematic functions

$$\begin{aligned} T_{\mathrm{a}_1,\mathrm{a}_1}(q_1^2,s) &= 4\big[\lambda(s,q_1^2,m_{f_1}^2)\big]^2, \\ T_{\mathrm{a}_2,\mathrm{a}_2}(q_1^2,s) &= m_{f_1}^6(s+q_1^2) - m_{f_1}^4(s^2+q_1^4-6sq_1^2) - m_{f_1}^2(s-q_1^2)^2(s+q_1^2) + (s-q_1^2)^4, \\ T_{\mathrm{s},\mathrm{s}}(q_1^2,s) &= m_{f_1}^2(s+q_1^2)\big(m_{f_1}^4 - s^2 - q_1^4 + 18sq_1^2\big) - m_{f_1}^4(s^2+q_1^4+14sq_1^2) + (s^2-q_1^4)^2, \\ T_{\mathrm{a}_1,\mathrm{a}_2}(q_1^2,s) &= 2\lambda(s,q_1^2,m_{f_1}^2)\big[(s-q_1^2)^2 - m_{f_1}^2(s+q_1^2)\big], \\ T_{\mathrm{a}_1,\mathrm{s}}(q_1^2,s) &= -2\lambda(s,q_1^2,m_{f_1}^2)(s-q_1^2)(s+q_1^2-m_{f_1}^2), \\ T_{\mathrm{a}_2,\mathrm{s}}(q_1^2,s) &= -(s-q_1^2)\Big[m_{f_1}^6 - m_{f_1}^4(s+q_1^2) - m_{f_1}^2(s^2+q_1^4-6sq_1^2) + (s-q_1^2)^2(s+q_1^2)\Big]. \end{aligned} \tag{4.24}$$

In a compact way, the cross section can be expressed in terms of the amputated helicity amplitudes [61]

$$\begin{aligned} \bar{H}_{++;0}(q_1^2,s) &= \frac{\lambda(s,q_1^2,m_{f_1}^2)}{2m_{f_1}^3}\bar{\mathcal{F}}_1(s) - \frac{q_1^2(m_{f_1}^2-q_1^2+s)}{2m_{f_1}^3}\bar{\mathcal{F}}_2(s) - \frac{s(m_{f_1}^2+q_1^2-s)}{2m_{f_1}^3}\bar{\mathcal{F}}_3(s), \\ \bar{H}_{+0;+}(q_1^2,s) &= \frac{q_1^2 s}{\xi_2 m_{f_1}^2}\bar{\mathcal{F}}_2(s) + \frac{s(m_{f_1}^2-q_1^2-s)}{2\xi_2 m_{f_1}^2}\bar{\mathcal{F}}_3(s), \\ \bar{H}_{0+;-}(q_1^2,s) &= -\frac{q_1^2(m_{f_1}^2-q_1^2-s)}{2\xi_1 m_{f_1}^2}\bar{\mathcal{F}}_2(s) - \frac{q_1^2 s}{\xi_1 m_{f_1}^2}\bar{\mathcal{F}}_3(s), \end{aligned} \tag{4.25}$$

with polarization-vector normalizations $\xi_1^2 = q_1^2$, $\xi_2^2 = s$, leading to

$$\sigma(e^+e^- \to f_1\rho)(s) = \frac{e^4|g_{\rho\gamma}|^2|\boldsymbol{p}_\rho|(s+2m_e^2)}{24\pi M_\rho^4 s^3|\boldsymbol{p}_e|}\sum_\lambda \big|\bar{H}_\lambda(M_\rho^2,s)\big|^2, \tag{4.26}$$

and the sum extends over the three amplitudes in eq. (4.25).

4.5 $e^+e^- \to f_1\pi^+\pi^-$

To obtain a reasonable threshold behavior, it is mandatory to go beyond the approximation of a narrow ρ and instead consider the full amplitude $e^+e^- \to f_1\pi^+\pi^-$. To this end, we use

$$\mathcal{M}(\rho \to \pi^+\pi^-) = g_{\rho\pi\pi}\epsilon_\mu(p_\rho)(p_- - p_+)^\mu \tag{4.27}$$

to calculate the diagram shown in figure 1, leading to

$$\begin{aligned}\mathcal{M}(e^+e^- \to f_1\pi^+\pi^-) = &\frac{e^2 g_{\rho\pi\pi}}{\tilde{g}_{\rho\gamma}m_{f_1}^2}\epsilon_\alpha^*(P)\frac{(p_- - p_+)_\mu}{q_1^2 - M_\rho^2 + iM_\rho\Gamma_\rho}\frac{\bar{v}^s(p_1)\gamma_\nu u^r(p_2)}{q_2^2} \\ &\times\Big[T_{\mathrm{a}_1}^{\mu\nu\alpha}(-q_1,q_2)\bar{\mathcal{F}}_{\mathrm{a}_1}(q_2^2) + T_{\mathrm{a}_2}^{\mu\nu\alpha}(-q_1,q_2)\bar{\mathcal{F}}_{\mathrm{a}_2}(q_2^2) + T_{\mathrm{s}}^{\mu\nu\alpha}(-q_1,q_2)\bar{\mathcal{F}}_{\mathrm{s}}(q_2^2)\Big],\end{aligned} \tag{4.28}$$

where we again dropped an unobservable phase. From the spin-averaged squared matrix element and after carrying out the angular integrations, we obtain the differential cross section

$$\begin{aligned}\frac{\mathrm{d}\sigma(e^+e^- \to f_1\pi^+\pi^-)}{\mathrm{d}q_1^2}(s) = &\frac{e^4|g_{\rho\pi\pi}|^2|g_{\rho\gamma}|^2|\boldsymbol{p}_\rho|(s+2m_e^2)(q_1^2-4M_\pi^2)^{3/2}}{18432\pi^3 m_{f_1}^6 M_\rho^4 s^3\sqrt{q_1^2}|\boldsymbol{p}_e|\big[(q_1^2-M_\rho^2)^2+M_\rho^2\Gamma_\rho^2\big]} \\ &\times\Big[T_{\mathrm{a}_1,\mathrm{a}_1}(q_1^2,s)\big|\bar{\mathcal{F}}_{\mathrm{a}_1}(s)\big|^2 + T_{\mathrm{a}_2,\mathrm{a}_2}(q_1^2,s)\big|\bar{\mathcal{F}}_{\mathrm{a}_2}(s)\big|^2 + T_{\mathrm{s},\mathrm{s}}(q_1^2,s)\big|\bar{\mathcal{F}}_{\mathrm{s}}(s)\big|^2 \\ &+ 2T_{\mathrm{a}_1,\mathrm{a}_2}(q_1^2,s)\mathrm{Re}\big[\bar{\mathcal{F}}_{\mathrm{a}_1}(s)\bar{\mathcal{F}}_{\mathrm{a}_2}^*(s)\big] + 2T_{\mathrm{a}_1,\mathrm{s}}(q_1^2,s)\mathrm{Re}\big[\bar{\mathcal{F}}_{\mathrm{a}_1}(s)\bar{\mathcal{F}}_{\mathrm{s}}^*(s)\big] \\ &+ 2T_{\mathrm{a}_2,\mathrm{s}}(q_1^2,s)\mathrm{Re}\big[\bar{\mathcal{F}}_{\mathrm{a}_2}(s)\bar{\mathcal{F}}_{\mathrm{s}}^*(s)\big]\Big],\end{aligned} \tag{4.29}$$

with the kinematic functions $T_{i,j}(q_1^2,s)$ as in eq. (4.24). In terms of the amputated helicity amplitudes, we obtain

$$\frac{\mathrm{d}\sigma(e^+e^- \to f_1\pi^+\pi^-)}{\mathrm{d}q_1^2}(s) = \frac{e^4|g_{\rho\pi\pi}|^2|g_{\rho\gamma}|^2|\boldsymbol{p}_\rho|(s+2m_e^2)(q_1^2-4M_\pi^2)^{3/2}}{1152\pi^3 M_\rho^4 s^3\sqrt{q_1^2}|\boldsymbol{p}_e|\big[(q_1^2-M_\rho^2)^2+M_\rho^2\Gamma_\rho^2\big]}\sum_\lambda\big|\bar{H}_\lambda(q_1^2,s)\big|^2. \tag{4.30}$$

In general, the remaining integration over q_1^2 needs to be performed numerically, but it is instructive to consider the limit of a narrow resonance [109]

$$\frac{1}{(q_1^2-M_\rho^2)^2+M_\rho^2\Gamma_\rho^2} \to \frac{\pi}{M_\rho\Gamma_\rho}\delta\big(q_1^2-M_\rho^2\big). \tag{4.31}$$

In this approximation, together with

$$\Gamma_\rho = \frac{|g_{\rho\pi\pi}|^2(M_\rho^2-4M_\pi^2)^{3/2}}{48\pi M_\rho^2}, \tag{4.32}$$

the q_1^2 integration of eq. (4.30) indeed reproduces eq. (4.26). For the phenomenological analysis of the $e^+e^- \to f_1\pi^+\pi^-$ data, we will use the full expression given in eq. (4.29).

JHEP08(2023)209

Quantity	Value	Reference
$\tilde{\Gamma}^{f_1}_{\gamma\gamma}$ [keV]	3.5(6)(5)	[69]
Λ_{f_1} [GeV]	1.04(6)(5)	[69]
$B(f_1 \to \rho\gamma)$	4.2(1.0)%	[62]
$r_{\rho\gamma}$	3.9(1.3)	[110]
$B(f_1 \to \phi\gamma)$	$0.74(26) \times 10^{-3}$	[111, 112]

Table 2. Data for $e^+e^- \to e^+e^- f_1$ and $f_1 \to V\gamma$ used in our analysis.

5 Phenomenological analysis

5.1 Data input for $e^+e^- \to e^+e^- f_1$ and $f_1 \to V\gamma$

The experimental data we will use for the space-like reaction $e^+e^- \to e^+e^- f_1$ and the radiative decays $f_1 \to V\gamma$ are summarized in table 2. For the former, this concerns normalization and slope from the L3 experiment [69], with isoscalar corrections evaluated using the mixing angle that follows from a combined analysis with the analogous quantities for the $f_1(1420)$ [70], see section 3. For $B(f_1 \to \rho\gamma)$, we use the results of the global fit from ref. [62], including data on $\Gamma(f_1 \to K\bar{K}\pi)/\Gamma(f_1 \to 4\pi)$ [113–115], $\Gamma(f_1 \to 4\pi)/\Gamma(f_1 \to \eta\pi\pi)$ [116, 117], $\Gamma(f_1 \to \rho\gamma)/\Gamma(f_1 \to 4\pi)$ [118], $\Gamma(f_1 \to a_0(980)\pi\,[\text{excluding } K\bar{K}\pi])/\Gamma(f_1 \to \eta\pi\pi)$ [116, 119, 120], $\Gamma(f_1 \to K\bar{K}\pi)/\Gamma(f_1 \to \eta\pi\pi)$ [92, 116, 119–122], and $\Gamma(f_1 \to \rho\gamma)/\Gamma(f_1 \to \eta\pi\pi)$ [92, 110, 120, 123]. As detailed in ref. [62], our fit differs from the PDG average, $B(f_1 \to \rho\gamma) = 6.1(1.0)\%$ [112], for two main reasons: we include the result from ref. [110], which reduces the average, and we set the fit up in terms of $\Gamma(f_1 \to \rho\gamma)/\Gamma(f_1 \to \eta\pi\pi)$ instead of $\Gamma(f_1 \to \eta\pi\pi)/\Gamma(f_1 \to \rho\gamma)$ as in ref. [112], since the latter introduces a bias towards larger branching fractions $B(f_1 \to \rho\gamma)$. For $B(f_1 \to \phi\gamma)$, there is a single measurement from ref. [111], and we will consider fit variants with and without this additional input, given both the tenuous data situation and the required $U(3)$ assumptions.[6] Finally, two event candidates for $f_1 \to e^+e^-$ have been observed in ref. [73], which, when interpreted as a signal, translates to $B(f_1 \to e^+e^-) = 5.1^{+3.7}_{-2.7} \times 10^{-9}$, while being quoted as $B(f_1 \to e^+e^-) < 9.4 \times 10^{-9}$ (90% C.L.) in ref. [112]. In ref. [62] we performed a detailed analysis of the constraints that can be obtained from the dilepton decay, but in view of its unclear status and large uncertainties, we no longer include this channel in our global fit here and instead focus on $e^+e^- \to f_1\pi^+\pi^-$. Further input parameters are collected in appendix A.

5.2 Data input for $e^+e^- \to f_1\pi^+\pi^-$

The process $e^+e^- \to f_1\pi^+\pi^-$ has been measured in two different decay channels, $f_1 \to \eta\pi\pi$ [74] and $f_1 \to K\bar{K}\pi$ [75]. The data for the cross section from both reconstruction methods are well compatible, indicating that systematic errors are smaller than the statistical uncertainties of the measurements. In the following, we will therefore assume that the data are indeed dominated by statistics.

[6] The limit $B(f_1 \to \phi\gamma) < 0.45 \times 10^{-3}$ [92, 112] (95% C.L.) supports a rather small branching fraction to $\phi\gamma$, indicating a value at the lower end of the range from ref. [111]. Both measurements are also consistent with $B(f_1 \to \phi\gamma) < 0.9 \times 10^{-3}$ [110] (95% C.L.).

JHEP08(2023)209

	$f_1 \to \phi\gamma$	
	No	Yes
χ^2/dof	$5.6/3 = 1.86$	$18.1/4 = 4.52$
p-value	0.13	1.2×10^{-3}
C_s	0.95(13)	0.76(16)
C_{a_1}	$-0.16(18)$	$-0.07(18)$
C_{a_2}	0.47(25)	0.09(32)
ρ_{sa_1}	0.34	0.31
ρ_{sa_2}	-0.11	-0.34
$\rho_{\text{a}_1\text{a}_2}$	-0.52	-0.35
$B(f_1 \to \phi\gamma) \times 10^3$	3.4(1.7)	1.6(1.0)
$B(f_1 \to \omega\gamma) \times 10^3$	5.5(1.6)	2.5(1.1)
$B(f_1 \to e^+e^-) \times 10^9$	2.2(6)	1.2(5)
$B(f_1' \to \phi\gamma) \times 10^3$	11.0(3.0)	5.2(2.2)
$B(f_1' \to \rho\gamma) \times 10^3$	4.8(2.6)	2.2(1.4)

Table 3. Best-fit results for the three VMD couplings C_s, C_{a_1}, and C_{a_2}. The fit includes the constraints from the normalization and slope measured by L3 in $e^+e^- \to e^+e^- f_1$, from $B(f_1 \to \rho\gamma)$, $r_{\rho\gamma}$, and $\sigma(e^+e^- \to f_1\pi^+\pi^-)$, as well as, in the right column, from $B(f_1 \to \phi\gamma)$. All uncertainties are inflated by the scale factor $S = \sqrt{\chi^2/\text{dof}}$. The table also shows the correlations ρ_{ij} among the three couplings and the values of $B(f_1 \to V\gamma)$, $V = \omega, \phi$, and $B(f_1 \to e^+e^-)$ implied by the fit result (the latter for $\sqrt{s_\text{m}} = 1.3\,\text{GeV}$). The uncertainties for $B(f_1 \to V\gamma)$ include the fit errors and ΔR^ϕ, but no additional estimate of $U(3)$ uncertainties. The predictions for $B(f_1' \to \phi\gamma)$ and $B(f_1' \to \rho\gamma)$ use the $U(3)$ relations from eq. (5.5).

Next, around $\sqrt{s} \simeq 2\,\text{GeV}$, the cross section displays resonance structures [88], most prominently the $\rho(2150)$, and, potentially, further excited ρ states. This implies that we cannot expect our theoretical description based on eq. (4.29) to provide an adequate fit to the data, because ρ excitations beyond the $\rho(1700)$ are not included. However, the data still provide a valuable upper bound for the background contributions that our TFF parameterizations do describe; in fact, this constraint proves extremely stringent, immediately ruling out, by at least an order of magnitude, parameterizations that do not implement the doubly-virtual asymptotic behavior of eq. (3.8). Even more, writing the cross section in terms of the couplings $C_{\text{a}_{1/2}}$, C_s, one observes that moderate cancellations among the different terms are required to obey the upper limit implied by the $e^+e^- \to f_1\pi^+\pi^-$ data. With C_s reasonably well determined from the L3 equivalent two-photon decay width, this thus implies a valuable constraint on the antisymmetric TFFs.

To quantify this constraint, we proceed as follows: we first define the χ^2 function

$$\chi^2_\text{BaBar}(C_\text{s}, C_{\text{a}_1}, C_{\text{a}_2}) = \sum_{i=1}^{n_\text{BaBar}} \frac{(\sigma(s_i, C_\text{s}, C_{\text{a}_1}, C_{\text{a}_2}) - \sigma_i^\text{exp})^2}{(\Delta\sigma_i^\text{exp})^2} \theta\big[\sigma(s_i, C_\text{s}, C_{\text{a}_1}, C_{\text{a}_2}) - \sigma_i^\text{exp}\big], \quad (5.1)$$

where $n_\text{BaBar} = 52$ is the combined number of data points from refs. [74, 75], σ_i^exp and $\Delta\sigma_i^\text{exp}$ are central value and error at center-of-mass energy $\sqrt{s_i}$, respectively, and the

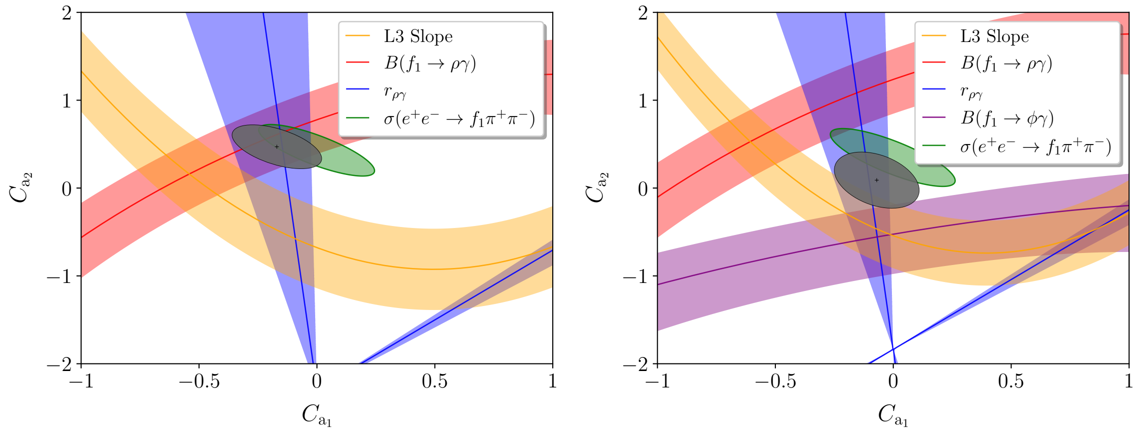

Figure 3. Left: constraints in the C_{a_1}–C_{a_2} plane for the respective best-fit value of C_s (see table 3), from L3 normalization and slope, $B(f_1 \to \rho\gamma)$, $r_{\rho\gamma}$, and $\sigma(e^+e^- \to f_1\pi^+\pi^-)$. The gray ellipse represents the result of the global fit. Right: same figure for the global fit including, in addition, $B(f_1 \to \phi\gamma)$.

Heaviside function demands that contributions to χ^2_{BaBar} only arise when the theoretical model exceeds the central value of the data, thus not penalizing a potential excess of the latter due to excited ρ resonances. Interpreting this χ^2 function in the usual statistical sense, however, puts an undue emphasis on the $e^+e^- \to f_1\pi^+\pi^-$ data, especially in view of the uncertainties from the contamination of resonant contributions. For this reason, we instead study contours in the C_{a_1}–C_{a_2} plane for which $\chi^2_{\text{BaBar}}/\text{dof} = 1$ at a given value of C_s, which should provide a reasonable measure of the consistency of the encompassed values of $C_{a_{1/2}}$ with the experimental constraints. We repeat this procedure for the relevant range of C_s and formulate the resulting constraint on $C_{a_{1/2}}$ in terms of an ellipse whose parameters are interpolated as a function of C_s. The final constraint is then written as

$$\chi^2_{\text{BaBar, eff}}(C_s, C_{a_1}, C_{a_2}) = \Delta\boldsymbol{y}_a^{\intercal} C_a^{-1} \Delta\boldsymbol{y}_a, \tag{5.2}$$

where

$$\Delta\boldsymbol{y}_a = \begin{pmatrix} C_{a_1} - C_{a_1}^{(0)} \\ C_{a_2} - C_{a_2}^{(0)} \end{pmatrix}, \tag{5.3}$$

with central values $C_{a_{1/2}}^{(0)}$ and covariance matrix C_a, determined via the $\chi^2_{\text{BaBar}}/\text{dof} = 1$ contour ellipse, implicitly depending on C_s. This effective χ^2 function defined in eq. (5.2) is then used as input in the global fit, counted as two data points in the number of degrees of freedom. This procedure is further motivated by the fact that the constraints imposed by the cross-section measurements at different energies will be highly correlated, since, if the upper limit is fulfilled at some point s_i for a set of couplings C_{a_1}, C_{a_2}, C_s, the smoothness of the cross section makes it likely that the same holds true at neighboring points as well.

5.3 Global fit

The results of the global fit are summarized in table 3, figure 3, and figure 4, for variants with and without the $U(3)$ constraint from $B(f_1 \to \phi\gamma)$. Without this input, we observe

JHEP08(2023)209

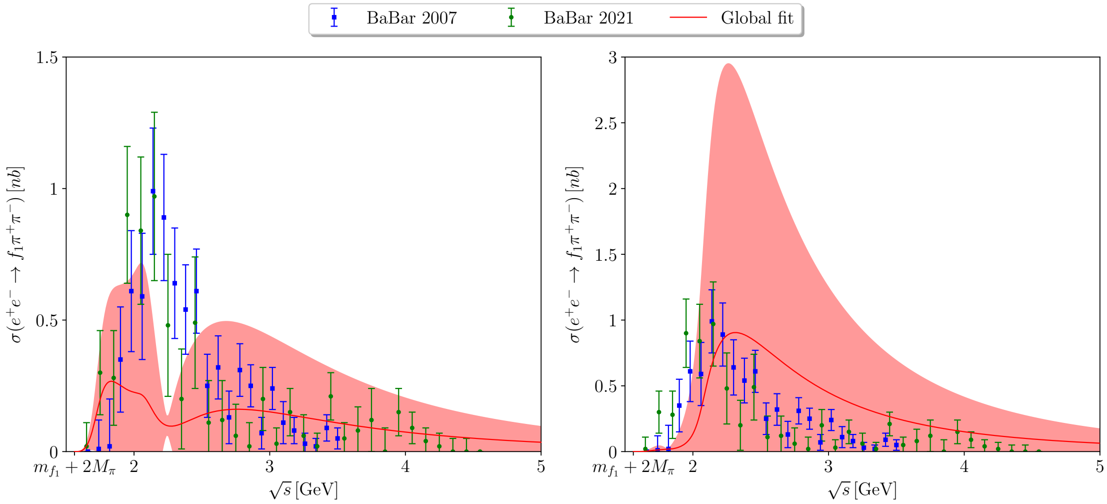

Figure 4. Comparison of our global fit results to the BaBar data [74, 75] for $\sigma(e^+e^- \to f_1\pi^+\pi^-)$, without (left) and including (right) the constraint from $B(f_1 \to \phi\gamma)$. The red line denotes the central result and the band reflects the uncertainties propagated from C_s, C_{a_1}, and C_{a_2}.

reasonable consistency among the various constraints, with a final value for C_s close to the L3 value in eq. (4.1). The coupling C_{a_1} comes out consistent with zero, while a non-zero value of C_{a_2} is obtained at 2σ significance. Crucially, owing to the inclusion of the BaBar data on $e^+e^- \to f_1\pi^+\pi^-$ [74, 75], we are now able to provide an unambiguous solution for all three TFFs, including the two antisymmetric ones encoded in $C_{\mathrm{a}_{1/2}}$. The best-fit point lies within the ellipse from $\sigma(e^+e^- \to f_1\pi^+\pi^-)$ and, accordingly, the central line in figure 4 respects the bound for almost all data points, leaving a deficit that could be well explained by a $\rho(2150)$-resonance signal. Moreover, the resulting prediction for $B(f_1 \to e^+e^-)$ is consistent with SND [73], suggesting a potential signal at the lower end of their range. In contrast, the prediction for $B(f_1 \to \phi\gamma)$ comes out slightly too large in comparison to ref. [111], in tension at the level of 1.5σ.

The same tension is visible in the global fit including $B(f_1 \to \phi\gamma)$, as the χ^2/dof deteriorates appreciably. Including the resulting scale factor $S = 2.1$ in the error estimates, all three couplings are consistent with the global fit without $B(f_1 \to \phi\gamma)$, but C_s decreases compared to L3 and the central value of C_{a_2} moves much closer to zero. Within the sizable uncertainties, the cross section for $e^+e^- \to f_1\pi^+\pi^-$ is still consistent, but the central line exceeds the data above the $\rho(2150)$, in accordance with the best-fit point in figure 3 lying slightly outside the $\sigma(e^+e^- \to f_1\pi^+\pi^-)$ ellipse. The resulting prediction for $B(f_1 \to e^+e^-)$ is still consistent with SND, and $B(f_1 \to \phi\gamma)$ now agrees by construction. Table 3 also includes the predictions for $B(f_1 \to \omega\gamma)$, $B(f_1' \to \phi\gamma)$, and $B(f_1' \to \rho\gamma)$, the latter two being related to the already determined couplings via the $U(3)$ arguments in section 5.4.

JHEP08(2023)209

5.4 Final representations

To summarize, we propose that the low-energy contributions to the TFFs of the f_1 be described by the parameterizations

$$
\begin{aligned}
\mathcal{F}_{\mathrm{a}_{1/2}}^{f_1,I=1}(q_1^2,q_2^2) &= \frac{R^\rho C_{\mathrm{a}_{1/2}}\zeta_\rho M_\rho^4 M_{\rho'}^4 M_{\rho''}^4(q_1^2-q_2^2)}{(q_1^2-M_\rho^2)(q_2^2-M_\rho^2)(q_1^2-M_{\rho'}^2)(q_2^2-M_{\rho'}^2)(q_1^2-M_{\rho''}^2)(q_2^2-M_{\rho''}^2)},\\
\mathcal{F}_{\mathrm{s}}^{f_1,I=1}(q_1^2,q_2^2) &= \frac{R^\rho C_{\mathrm{s}} M_\rho^4 M_{\rho'}^4}{(q_1^2-M_\rho^2)(q_2^2-M_\rho^2)(q_1^2-M_{\rho'}^2)(q_2^2-M_{\rho'}^2)},\\
\mathcal{F}_{\mathrm{a}_{1/2}}^{f_1,I=0}(q_1^2,q_2^2) &= \sum_{V=\omega,\phi}\frac{R^V C_{\mathrm{a}_{1/2}}\zeta_V M_V^4 M_{V'}^4 M_{V''}^4(q_1^2-q_2^2)}{(q_1^2-M_V^2)(q_2^2-M_V^2)(q_1^2-M_{V'}^2)(q_2^2-M_{V'}^2)(q_1^2-M_{V''}^2)(q_2^2-M_{V''}^2)},\\
\mathcal{F}_{\mathrm{s}}^{f_1,I=0}(q_1^2,q_2^2) &= \sum_{V=\omega,\phi}\frac{R^V C_{\mathrm{s}} M_V^4 M_{V'}^4}{(q_1^2-M_V^2)(q_2^2-M_V^2)(q_1^2-M_{V'}^2)(q_2^2-M_{V'}^2)},
\end{aligned}
\tag{5.4}
$$

see eq. (3.6), eq. (3.7), eq. (3.10), and eq. (3.11), with couplings C_{s}, C_{a_1}, and C_{a_2} as determined in table 3 (and $R^\rho = 1$). These low-energy contributions are then to be supplemented by the asymptotic contributions from the LCE, see section 2, to arrive at a complete description.

In order to estimate the impact of f_1' and a_1, we also quote the corresponding expressions that follow from $U(3)$ symmetry. For the f_1', the analogous results are obtained by replacing

$$
\begin{aligned}
R^\rho \to R^\rho_{f_1'} &= \cot(\theta_A+\theta_1) = -0.50(11),\\
R^\omega \to R^\omega_{f_1'} &= \frac{1}{9}\cot(\theta_A+\theta_1) = -0.06(1),\\
R^\phi \to R^\phi_{f_1'} &= -\frac{2\sqrt{2}}{9} = -0.31,
\end{aligned}
\tag{5.5}
$$

where the errors only refer to the uncertainties propagated in θ_A, cf. eq. (3.2) and eq. (3.11). The coefficients in eq. (5.5) show that isoscalar contributions will become much more important for the f_1' than for the f_1, especially the ϕ. This observation is reflected by some evidence for a signal in the decay to the $\phi\gamma$ final state, $B(f_1'\to\phi\gamma) = 3(2)\times 10^{-3}$ [92], which, within uncertainties, agrees with the predictions from table 3 for the fit including $B(f_1\to\phi\gamma)$, while the fit without $B(f_1\to\phi\gamma)$ predicts a larger branching fraction. The same reference also gives a limit $B(f_1'\to\rho\gamma) < 0.02$ (95% C.L.), in agreement with both fits from table 3.

The TFFs of the a_1 display a different isospin structure, with one isoscalar and one isovector photon each. Moreover, for ideal mixing, there is no contribution from the ϕ and its excitations, so that only contributions of the ρ–ω type survive. Accordingly, the overall scaling compared to the couplings in the f_1 TFFs is measured relative to the sum of all isovector and isoscalar contributions, leading to

$$
R_{a_1} = \frac{1+R^\omega+R^\phi}{\sqrt{3}\cos(\theta_A-\theta_0)} = \frac{2}{3\sin(\theta_A+\theta_1)} = 0.75(3). \tag{5.6}
$$

Choosing a symmetric decomposition of ζ_V onto the ρ and ω contributions, we obtain

$$\begin{aligned}
\mathcal{F}^{a_1}_{\mathrm{a}_{1/2}}(q_1^2,q_2^2) &= \frac{R_{a_1} C_{\mathrm{a}_{1/2}} \sqrt{\zeta_\rho\zeta_\omega} M_\rho^2 M_{\rho'}^2 M_{\rho''}^2 M_\omega^2 M_{\omega'}^2 M_{\omega''}^2 (q_1^2-q_2^2)}{2(q_1^2-M_\rho^2)(q_2^2-M_\omega^2)(q_1^2-M_{\rho'}^2)(q_2^2-M_{\omega'}^2)(q_1^2-M_{\rho''}^2)(q_2^2-M_{\omega''}^2)} \\
&\quad + (\rho\leftrightarrow\omega), \\
\mathcal{F}^{a_1}_{\mathrm{s}}(q_1^2,q_2^2) &= \frac{R_{a_1} C_{\mathrm{s}} M_\rho^2 M_{\rho'}^2 M_\omega^2 M_{\omega'}^2}{2(q_1^2-M_\rho^2)(q_2^2-M_\omega^2)(q_1^2-M_{\rho'}^2)(q_2^2-M_{\omega'}^2)} + (\rho\leftrightarrow\omega).
\end{aligned} \tag{5.7}$$

6 Conclusions

The transition form factors (TFFs) of axial-vector mesons are key input quantities for a data-driven evaluation of hadronic light-by-light (HLbL) scattering in the anomalous magnetic moment of the muon, yet they are notoriously poorly determined from experiment. Here, we performed a global analysis of all experimental constraints available for the $f_1(1285)$ and outlined how the $f_1(1420)$ and $a_1(1260)$ contributions can be estimated from $U(3)$ symmetry. A crucial role is played by data for the cross section of $e^+e^-\to f_1\pi^+\pi^-$, which provide valuable input on the asymptotic behavior and allowed us to find an unambiguous solution also for the antisymmetric TFFs.

The process $e^+e^-\to f_1\pi^+\pi^-$ probes all three TFFs at one photon virtuality determined by the center-of-mass energy and the other one by the $\pi^+\pi^-$ invariant mass, which in turn is dominated by the $\rho(770)$. Accordingly, the data extending from threshold up to about 4.5 GeV are sensitive to the asymptotic behavior for one virtuality fixed at the ρ mass. The corresponding constraint demonstrates that the asymptotic behavior predicted by the light-cone expansion needs to set in early, for otherwise, the cross section exceeds data by an order of magnitude. We implemented this conclusion using a vector-meson-dominance ansatz, leading to the parameterizations summarized in section 5.4. To account for contributions from even higher excited ρ resonances, such as the $\rho(2150)$, we formulated the quantitative analysis as an upper limit, which still entails valuable constraints especially on the otherwise poorly determined couplings characterizing the antisymmetric TFFs. The global fit, see section 5.3, shows good consistency with data for $e^+e^-\to e^+e^-f_1$ and $f_1\to\rho\gamma$, predicting a branching fraction for $f_1\to e^+e^-$ at the lower end of the signal strength reported by SND. Some tension is observed with $f_1\to\phi\gamma$, which might point towards limitations of $U(3)$ symmetry and/or the data base.

The final parameterizations describe the TFFs at low and intermediate virtualities, to be supplemented by an additional term from the light-cone expansion [61, 62] that ensures the correct asymptotic behavior also in the doubly-virtual direction. Using this combined input, work is ongoing to evaluate the axial-vector contributions both in the HLbL basis of ref. [55] and in the formalism of ref. [60]. In combination with the short-distance constraints from refs. [47–49], the results presented here will thus be instrumental to arrive at a complete data-driven evaluation of HLbL scattering and to reduce the uncertainties to the level required by the final precision expected from the Fermilab experiment.

JHEP08(2023)209

Acknowledgments

We thank Peter Stoffer for useful comments on the manuscript. Financial support by the DFG through the funds provided to the Sino-German Collaborative Research Center TRR110 "Symmetries and the Emergence of Structure in QCD" (DFG Project-ID 196253076 – TRR 110) and the SNSF (Project No. PCEFP2_181117) is gratefully acknowledged.

A Constants and parameters

In table 4, we collect the masses and decay widths used in this work, in large part taken from ref. [112]. For most quantities, possible effects from isospin breaking can be safely neglected, but some ambiguity arises for the mass and width of the $\rho(770)$. For the $e^+e^- \to f_1\pi^+\pi^-$ process as the focus of this work, it would be natural to identify the ρ parameters with the ρ^0, whose width is quoted at an appreciably lower value than for the charged channel. However, here we follow the arguments from ref. [62], observing that determinations sensitive also to the excited ρ states both in the neutral [124] and charged mode [125] tend to support the charged-channel values from ref. [112] and, therefore, use the latter ones throughout. In particular, via eq. (4.32), this determines $|g_{\rho\pi\pi}| = 5.98$, in good agreement with dispersive determinations [108, 126]. Similarly, the photon couplings are calculated from eq. (4.20) with the branching fractions from ref. [112], leading to

$$|g_{\rho\gamma}| = 4.96, \qquad |g_{\omega\gamma}| = 16.51, \qquad |g_{\phi\gamma}| = 13.40. \tag{A.1}$$

Finally, we quote the values for masses and decay widths of the axial-vector resonances from ref. [112]. For the a_1, the (reaction-dependent) Breit–Wigner parameters can also be compared to attempts to extract the pole position from $\tau \to 3\pi\nu_\tau$ data, $\sqrt{s_{a_1}} = m_{a_1} - i\Gamma_{a_1}/2 = \big[1209(4)(^{+12}_{-9}) - i288(6)(^{+45}_{-10})\big]\,\text{MeV}$ [127]. In addition, ref. [112] quotes the average $\Gamma_{a_1} = 420(35)\,\text{MeV}$ [128, 129], in line with the center of the estimated range quoted in table 4. Based on the same two references, one would conclude the mass average $m_{a_1} = 1250(20)\,\text{MeV}$.

Quantity	Variable	Value	Reference
Mass pion	M_π	139.57 MeV	
Mass $f_1(1285)$	m_{f_1}	1281.9(5) MeV	
Mass $f_1(1420)$	$m_{f_1'}$	1426.3(9) MeV	
Mass $a_1(1260)$	m_{a_1}	1230(40) MeV	
Mass $\omega(782)$	M_ω	782.66(13) MeV	
Mass $\omega(1420)$	$M_{\omega'}$	1410(60) MeV	
Mass $\omega(1650)$	$M_{\omega''}$	1670(30) MeV	
Mass $\phi(1020)$	M_ϕ	1019.461(16) MeV	
Mass $\phi(1680)$	$M_{\phi'}$	1680(20) MeV	
Mass $\phi(2170)$	$M_{\phi''}$	2163(7) MeV	[112]
Mass $\rho(770)$ (charged)	M_ρ	775.11(34) MeV	
Mass $\rho(1450)$	$M_{\rho'}$	1465(25) MeV	
Mass $\rho(1700)$	$M_{\rho''}$	1720(20) MeV	
Total width $f_1(1285)$	Γ_{f_1}	22.7(1.1) MeV	
Total width $f_1(1420)$	$\Gamma_{f_1'}$	54.5(2.6) MeV	
Total width $a_1(1260)$	Γ_{a_1}	$(250\dots600)$ MeV	
Total width $\rho(770)$ (charged)	Γ_ρ	149.1(8) MeV	
Total width $\rho(1450)$	$\Gamma_{\rho'}$	400(60) MeV	
Total width $\rho(1700)$	$\Gamma_{\rho''}$	250(100) MeV	
Mass $\rho(770)$ (charged)	M_ρ	774.9(6) MeV	
Mass $\rho(1450)$ (charged)	$M_{\rho'}$	1428(30) MeV	
Mass $\rho(1700)$ (charged)	$M_{\rho''}$	1694(98) MeV	[124]
Total width $\rho(770)$ (charged)	Γ_ρ	148.6(1.8) MeV	
Total width $\rho(1450)$ (charged)	$\Gamma_{\rho'}$	413(58) MeV	
Total width $\rho(1700)$ (charged)	$\Gamma_{\rho''}$	135(62) MeV	
Mass $\rho(770)$ (neutral)	M_ρ	775.02(35) MeV	
Mass $\rho(1450)$ (neutral)	$M_{\rho'}$	1493(15) MeV	
Mass $\rho(1700)$ (neutral)	$M_{\rho''}$	1861(17) MeV	[125]
Total width $\rho(770)$ (neutral)	Γ_ρ	149.59(67) MeV	
Total width $\rho(1450)$ (neutral)	$\Gamma_{\rho'}$	427(31) MeV	
Total width $\rho(1700)$ (neutral)	$\Gamma_{\rho''}$	316(26) MeV	

Table 4. Masses and decay widths from ref. [112] as used in this work (first panel), in comparison to the $\rho(770)$, $\rho(1450)$, and $\rho(1700)$ parameters from refs. [124, 125].

JHEP08(2023)209

References

[1] T. Aoyama et al., *The anomalous magnetic moment of the muon in the Standard Model*, *Phys. Rept.* **887** (2020) 1 [arXiv:2006.04822] [INSPIRE].

[2] T. Aoyama, M. Hayakawa, T. Kinoshita and M. Nio, *Complete Tenth-Order QED Contribution to the Muon $g-2$*, *Phys. Rev. Lett.* **109** (2012) 111808 [arXiv:1205.5370] [INSPIRE].

[3] T. Aoyama, T. Kinoshita and M. Nio, *Theory of the Anomalous Magnetic Moment of the Electron*, *Atoms* **7** (2019) 28 [INSPIRE].

[4] A. Czarnecki, W.J. Marciano and A. Vainshtein, *Refinements in electroweak contributions to the muon anomalous magnetic moment*, *Phys. Rev. D* **67** (2003) 073006 [*Erratum ibid.* **73** (2006) 119901] [hep-ph/0212229] [INSPIRE].

[5] C. Gnendiger, D. Stöckinger and H. Stöckinger-Kim, *The electroweak contributions to $(g-2)_\mu$ after the Higgs boson mass measurement*, *Phys. Rev. D* **88** (2013) 053005 [arXiv:1306.5546] [INSPIRE].

[6] M. Davier, A. Hoecker, B. Malaescu and Z. Zhang, *Reevaluation of the hadronic vacuum polarisation contributions to the Standard Model predictions of the muon $g-2$ and $\alpha(m_Z^2)$ using newest hadronic cross-section data*, *Eur. Phys. J. C* **77** (2017) 827 [arXiv:1706.09436] [INSPIRE].

[7] A. Keshavarzi, D. Nomura and T. Teubner, *Muon $g-2$ and $\alpha(M_Z^2)$: a new data-based analysis*, *Phys. Rev. D* **97** (2018) 114025 [arXiv:1802.02995] [INSPIRE].

[8] G. Colangelo, M. Hoferichter and P. Stoffer, *Two-pion contribution to hadronic vacuum polarization*, *JHEP* **02** (2019) 006 [arXiv:1810.00007] [INSPIRE].

[9] M. Hoferichter, B.-L. Hoid and B. Kubis, *Three-pion contribution to hadronic vacuum polarization*, *JHEP* **08** (2019) 137 [arXiv:1907.01556] [INSPIRE].

[10] M. Davier, A. Hoecker, B. Malaescu and Z. Zhang, *A new evaluation of the hadronic vacuum polarisation contributions to the muon anomalous magnetic moment and to $\alpha(m_Z^2)$*, *Eur. Phys. J. C* **80** (2020) 241 [*Erratum ibid.* **80** (2020) 410] [arXiv:1908.00921] [INSPIRE].

[11] A. Keshavarzi, D. Nomura and T. Teubner, *$g-2$ of charged leptons, $\alpha(M_Z^2)$, and the hyperfine splitting of muonium*, *Phys. Rev. D* **101** (2020) 014029 [arXiv:1911.00367] [INSPIRE].

[12] B.-L. Hoid, M. Hoferichter and B. Kubis, *Hadronic vacuum polarization and vector-meson resonance parameters from $e^+e^- \to \pi^0\gamma$*, *Eur. Phys. J. C* **80** (2020) 988 [arXiv:2007.12696] [INSPIRE].

[13] A. Kurz, T. Liu, P. Marquard and M. Steinhauser, *Hadronic contribution to the muon anomalous magnetic moment to next-to-next-to-leading order*, *Phys. Lett. B* **734** (2014) 144 [arXiv:1403.6400] [INSPIRE].

[14] K. Melnikov and A. Vainshtein, *Hadronic light-by-light scattering contribution to the muon anomalous magnetic moment revisited*, Phys. Rev. D **70** (2004) 113006 [hep-ph/0312226] [INSPIRE].

[15] G. Colangelo, M. Hoferichter, M. Procura and P. Stoffer, *Dispersive approach to hadronic light-by-light scattering*, JHEP **09** (2014) 091 [arXiv:1402.7081] [INSPIRE].

[16] G. Colangelo et al., *Towards a data-driven analysis of hadronic light-by-light scattering*, Phys. Lett. B **738** (2014) 6 [arXiv:1408.2517] [INSPIRE].

[17] G. Colangelo, M. Hoferichter, M. Procura and P. Stoffer, *Dispersion relation for hadronic light-by-light scattering: theoretical foundations*, JHEP **09** (2015) 074 [arXiv:1506.01386] [INSPIRE].

[18] P. Masjuan and P. Sánchez-Puertas, *Pseudoscalar-pole contribution to the* $(g_\mu - 2)$*: a rational approach*, Phys. Rev. D **95** (2017) 054026 [arXiv:1701.05829] [INSPIRE].

[19] G. Colangelo, M. Hoferichter, M. Procura and P. Stoffer, *Rescattering effects in the hadronic-light-by-light contribution to the anomalous magnetic moment of the muon*, Phys. Rev. Lett. **118** (2017) 232001 [arXiv:1701.06554] [INSPIRE].

[20] G. Colangelo, M. Hoferichter, M. Procura and P. Stoffer, *Dispersion relation for hadronic light-by-light scattering: two-pion contributions*, JHEP **04** (2017) 161 [arXiv:1702.07347] [INSPIRE].

[21] M. Hoferichter et al., *Pion-pole contribution to hadronic light-by-light scattering in the anomalous magnetic moment of the muon*, Phys. Rev. Lett. **121** (2018) 112002 [arXiv:1805.01471] [INSPIRE].

[22] M. Hoferichter et al., *Dispersion relation for hadronic light-by-light scattering: pion pole*, JHEP **10** (2018) 141 [arXiv:1808.04823] [INSPIRE].

[23] A. Gérardin, H.B. Meyer and A. Nyffeler, *Lattice calculation of the pion transition form factor with* $N_f = 2 + 1$ *Wilson quarks*, Phys. Rev. D **100** (2019) 034520 [arXiv:1903.09471] [INSPIRE].

[24] J. Bijnens, N. Hermansson-Truedsson and A. Rodríguez-Sánchez, *Short-distance constraints for the HLbL contribution to the muon anomalous magnetic moment*, Phys. Lett. B **798** (2019) 134994 [arXiv:1908.03331] [INSPIRE].

[25] G. Colangelo et al., *Short-distance constraints on hadronic light-by-light scattering in the anomalous magnetic moment of the muon*, Phys. Rev. D **101** (2020) 051501 [arXiv:1910.11881] [INSPIRE].

[26] G. Colangelo et al., *Longitudinal short-distance constraints for the hadronic light-by-light contribution to* $(g-2)_\mu$ *with large-*N_c *Regge models*, JHEP **03** (2020) 101 [arXiv:1910.13432] [INSPIRE].

[27] T. Blum et al., *Hadronic Light-by-Light Scattering Contribution to the Muon Anomalous Magnetic Moment from Lattice QCD*, Phys. Rev. Lett. **124** (2020) 132002 [arXiv:1911.08123] [INSPIRE].

[28] G. Colangelo et al., *Remarks on higher-order hadronic corrections to the muon* $g-2$, Phys. Lett. B **735** (2014) 90 [arXiv:1403.7512] [INSPIRE].

[29] V. Pauk and M. Vanderhaeghen, *Single meson contributions to the muon's anomalous magnetic moment*, Eur. Phys. J. C **74** (2014) 3008 [arXiv:1401.0832] [INSPIRE].

JHEP08(2023)209

[30] I. Danilkin and M. Vanderhaeghen, *Light-by-light scattering sum rules in light of new data*, *Phys. Rev. D* **95** (2017) 014019 [arXiv:1611.04646] [INSPIRE].

[31] F. Jegerlehner, *The Anomalous Magnetic Moment of the Muon*, Springer (2017) [DOI:10.1007/978-3-319-63577-4] [INSPIRE].

[32] M. Knecht, S. Narison, A. Rabemananjara and D. Rabetiarivony, *Scalar meson contributions to a_μ from hadronic light-by-light scattering*, *Phys. Lett. B* **787** (2018) 111 [arXiv:1808.03848] [INSPIRE].

[33] G. Eichmann, C.S. Fischer and R. Williams, *Kaon-box contribution to the anomalous magnetic moment of the muon*, *Phys. Rev. D* **101** (2020) 054015 [arXiv:1910.06795] [INSPIRE].

[34] P. Roig and P. Sánchez-Puertas, *Axial-vector exchange contribution to the hadronic light-by-light piece of the muon anomalous magnetic moment*, *Phys. Rev. D* **101** (2020) 074019 [arXiv:1910.02881] [INSPIRE].

[35] MUON $g-2$ collaboration, *Measurement of the Positive Muon Anomalous Magnetic Moment to 0.46 ppm*, *Phys. Rev. Lett.* **126** (2021) 141801 [arXiv:2104.03281] [INSPIRE].

[36] MUON $g-2$ collaboration, *Magnetic-field measurement and analysis for the Muon $g-2$ Experiment at Fermilab*, *Phys. Rev. A* **103** (2021) 042208 [arXiv:2104.03201] [INSPIRE].

[37] MUON $g-2$ collaboration, *Beam dynamics corrections to the Run-1 measurement of the muon anomalous magnetic moment at Fermilab*, *Phys. Rev. Accel. Beams* **24** (2021) 044002 [arXiv:2104.03240] [INSPIRE].

[38] MUON $g-2$ collaboration, *Measurement of the anomalous precession frequency of the muon in the Fermilab Muon $g-2$ Experiment*, *Phys. Rev. D* **103** (2021) 072002 [arXiv:2104.03247] [INSPIRE].

[39] MUON $g-2$ collaboration, *Final Report of the Muon E821 Anomalous Magnetic Moment Measurement at BNL*, *Phys. Rev. D* **73** (2006) 072003 [hep-ex/0602035] [INSPIRE].

[40] MUON $g-2$ collaboration, *Muon $g-2$ Technical Design Report*, arXiv:1501.06858 [INSPIRE].

[41] G. Colangelo et al., *Prospects for precise predictions of a_μ in the Standard Model*, arXiv:2203.15810 [INSPIRE].

[42] E.-H. Chao et al., *Hadronic light-by-light contribution to $(g-2)_\mu$ from lattice QCD: a complete calculation*, *Eur. Phys. J. C* **81** (2021) 651 [arXiv:2104.02632] [INSPIRE].

[43] E.-H. Chao et al., *The charm-quark contribution to light-by-light scattering in the muon $(g-2)$ from lattice QCD*, *Eur. Phys. J. C* **82** (2022) 664 [arXiv:2204.08844] [INSPIRE].

[44] T. Blum et al., *Hadronic light-by-light contribution to the muon anomaly from lattice QCD with infinite volume QED at physical pion mass*, arXiv:2304.04423 [INSPIRE].

[45] C. Alexandrou et al., *The $\eta \to \gamma^*\gamma^*$ transition form factor and the hadronic light-by-light η-pole contribution to the muon $g-2$ from lattice QCD*, arXiv:2212.06704 [INSPIRE].

[46] A. Gérardin et al., *Lattice calculation of the π^0, η and η' transition form factors and the hadronic light-by-light contribution to the muon $g-2$*, arXiv:2305.04570 [INSPIRE].

[47] J. Bijnens, N. Hermansson-Truedsson, L. Laub and A. Rodríguez-Sánchez, *Short-distance HLbL contributions to the muon anomalous magnetic moment beyond perturbation theory*, *JHEP* **10** (2020) 203 [arXiv:2008.13487] [INSPIRE].

JHEP08(2023)209

[48] J. Bijnens, N. Hermansson-Truedsson, L. Laub and A. Rodríguez-Sánchez, *The two-loop perturbative correction to the $(g-2)_\mu$ HLbL at short distances*, JHEP **04** (2021) 240 [arXiv:2101.09169] [INSPIRE].

[49] J. Bijnens, N. Hermansson-Truedsson and A. Rodríguez-Sánchez, *Constraints on the hadronic light-by-light in the Melnikov-Vainshtein regime*, JHEP **02** (2023) 167 [arXiv:2211.17183] [INSPIRE].

[50] J. Leutgeb and A. Rebhan, *Axial vector transition form factors in holographic QCD and their contribution to the anomalous magnetic moment of the muon*, Phys. Rev. D **101** (2020) 114015 [arXiv:1912.01596] [INSPIRE].

[51] L. Cappiello et al., *Axial-vector and pseudoscalar mesons in the hadronic light-by-light contribution to the muon $(g-2)$*, Phys. Rev. D **102** (2020) 016009 [arXiv:1912.02779] [INSPIRE].

[52] M. Knecht, *On some short-distance properties of the fourth-rank hadronic vacuum polarization tensor and the anomalous magnetic moment of the muon*, JHEP **08** (2020) 056 [arXiv:2005.09929] [INSPIRE].

[53] P. Masjuan, P. Roig and P. Sánchez-Puertas, *The interplay of transverse degrees of freedom and axial-vector mesons with short-distance constraints in $g-2$*, J. Phys. G **49** (2022) 015002 [arXiv:2005.11761] [INSPIRE].

[54] J. Lüdtke and M. Procura, *Effects of longitudinal short-distance constraints on the hadronic light-by-light contribution to the muon $g-2$*, Eur. Phys. J. C **80** (2020) 1108 [arXiv:2006.00007] [INSPIRE].

[55] G. Colangelo et al., *Short-distance constraints for the longitudinal component of the hadronic light-by-light amplitude: an update*, Eur. Phys. J. C **81** (2021) 702 [arXiv:2106.13222] [INSPIRE].

[56] J. Leutgeb, J. Mager and A. Rebhan, *Hadronic light-by-light contribution to the muon $g-2$ from holographic QCD with solved $\mathrm{U}(1)_A$ problem*, Phys. Rev. D **107** (2023) 054021 [arXiv:2211.16562] [INSPIRE].

[57] M. Hoferichter and P. Stoffer, *Dispersion relations for $\gamma^*\gamma^* \to \pi\pi$: helicity amplitudes, subtractions, and anomalous thresholds*, JHEP **07** (2019) 073 [arXiv:1905.13198] [INSPIRE].

[58] I. Danilkin, M. Hoferichter and P. Stoffer, *A dispersive estimate of scalar contributions to hadronic light-by-light scattering*, Phys. Lett. B **820** (2021) 136502 [arXiv:2105.01666] [INSPIRE].

[59] S. Holz, C. Hanhart, M. Hoferichter and B. Kubis, *A dispersive analysis of $\eta' \to \pi^+\pi^-\gamma$ and $\eta' \to \ell^+\ell^-\gamma$*, Eur. Phys. J. C **82** (2022) 434 [*Addendum ibid.* **82** (2022) 1159] [arXiv:2202.05846] [INSPIRE].

[60] J. Lüdtke, M. Procura and P. Stoffer, *Dispersion relations for hadronic light-by-light scattering in triangle kinematics*, JHEP **04** (2023) 125 [arXiv:2302.12264] [INSPIRE].

[61] M. Hoferichter and P. Stoffer, *Asymptotic behavior of meson transition form factors*, JHEP **05** (2020) 159 [arXiv:2004.06127] [INSPIRE].

[62] M. Zanke, M. Hoferichter and B. Kubis, *On the transition form factors of the axial-vector resonance $f_1(1285)$ and its decay into e^+e^-*, JHEP **07** (2021) 106 [arXiv:2103.09829] [INSPIRE].

[63] L.D. Landau, *On the angular momentum of a system of two photons*, *Dokl. Akad. Nauk SSSR* **60** (1948) 207 [INSPIRE].

[64] C.-N. Yang, *Selection Rules for the Dematerialization of a Particle Into Two Photons*, *Phys. Rev.* **77** (1950) 242 [INSPIRE].

[65] G. Gidal et al., *Observation of spin-1 $f_1(1285)$ in the Reaction $\gamma\gamma^* \to \eta^0\pi^+\pi^-$*, *Phys. Rev. Lett.* **59** (1987) 2012 [INSPIRE].

[66] G. Gidal et al., *Observation of a Spin 1 Resonance in the Reaction $\gamma\gamma^* \to K^0K^\pm\pi^\mp$*, *Phys. Rev. Lett.* **59** (1987) 2016 [INSPIRE].

[67] TPC/Two Gamma collaboration, *Formation of Spin One Mesons by Photon-photon Fusion*, *Phys. Rev. D* **38** (1988) 1 [INSPIRE].

[68] TPC/Two Gamma collaboration, *$f_1(1285)$ formation in photon photon fusion reactions*, *Phys. Lett. B* **209** (1988) 107 [INSPIRE].

[69] L3 collaboration, *$f_1(1285)$ formation in two photon collisions at LEP*, *Phys. Lett. B* **526** (2002) 269 [hep-ex/0110073] [INSPIRE].

[70] L3 collaboration, *Study of resonance formation in the mass region 1400 MeV to 1500 MeV through the reaction $\gamma\gamma \to K^0_S K^\pm\pi^\mp$*, *JHEP* **03** (2007) 018 [INSPIRE].

[71] A.S. Rudenko, *$f_1(1285) \to e^+e^-$ decay and direct f_1 production in e^+e^- collisions*, *Phys. Rev. D* **96** (2017) 076004 [arXiv:1707.00545] [INSPIRE].

[72] A.I. Milstein and A.S. Rudenko, *Consistent analysis of $f_1(1285)$ meson form factors*, *Phys. Lett. B* **800** (2020) 135117 [arXiv:1909.07938] [INSPIRE].

[73] SND collaboration, *Search for direct production of the $f_1(1285)$ resonance in e^+e^- collisions*, *Phys. Lett. B* **800** (2020) 135074 [arXiv:1906.03838] [INSPIRE].

[74] BaBar collaboration, *The $e^+e^- \to 2(\pi^+\pi^-)\pi^0$, $2(\pi^+\pi^-)\eta$, $K^+K^-\pi^+\pi^-\pi^0$ and $K^+K^-\pi^+\pi^-\eta$ Cross Sections Measured with Initial-State Radiation*, *Phys. Rev. D* **76** (2007) 092005 [*Erratum ibid.* **77** (2008) 119902] [arXiv:0708.2461] [INSPIRE].

[75] BaBar collaboration, *Study of the reactions $e^+e^- \to K^+K^-\pi^0\pi^0\pi^0$, $e^+e^- \to K^0_S K^\pm\pi^\mp\pi^0\pi^0$, and $e^+e^- \to K^0_S K^\pm\pi^\mp\pi^+\pi^-$ at center-of-mass energies from threshold to 4.5 GeV using initial-state radiation*, *Phys. Rev. D* **107** (2023) 072001 [arXiv:2207.10340] [INSPIRE].

[76] D. Stamen et al., *Kaon electromagnetic form factors in dispersion theory*, *Eur. Phys. J. C* **82** (2022) 432 [arXiv:2202.11106] [INSPIRE].

[77] G. Colangelo et al., *Data-driven evaluations of Euclidean windows to scrutinize hadronic vacuum polarization*, *Phys. Lett. B* **833** (2022) 137313 [arXiv:2205.12963] [INSPIRE].

[78] G. Colangelo, M. Hoferichter, B. Kubis and P. Stoffer, *Isospin-breaking effects in the two-pion contribution to hadronic vacuum polarization*, *JHEP* **10** (2022) 032 [arXiv:2208.08993] [INSPIRE].

[79] M. Hoferichter et al., *A phenomenological estimate of isospin breaking in hadronic vacuum polarization*, arXiv:2307.02532 [INSPIRE].

[80] M. Hoferichter, B.-L. Hoid, B. Kubis and D. Schuh, *Isospin-breaking effects in the three-pion contribution to hadronic vacuum polarization*, arXiv:2307.02546 [INSPIRE].

[81] S. Borsanyi et al., *Leading hadronic contribution to the muon magnetic moment from lattice QCD*, *Nature* **593** (2021) 51 [arXiv:2002.12347] [INSPIRE].

JHEP08(2023)209

[82] M. Cè et al., *Window observable for the hadronic vacuum polarization contribution to the muon $g-2$ from lattice QCD*, *Phys. Rev. D* **106** (2022) 114502 [arXiv:2206.06582] [INSPIRE].

[83] Extended Twisted Mass collaboration, *Lattice calculation of the short and intermediate time-distance hadronic vacuum polarization contributions to the muon magnetic moment using twisted-mass fermions*, *Phys. Rev. D* **107** (2023) 074506 [arXiv:2206.15084] [INSPIRE].

[84] Fermilab Lattice et al. collaborations, *Light-quark connected intermediate-window contributions to the muon $g-2$ hadronic vacuum polarization from lattice QCD*, *Phys. Rev. D* **107** (2023) 114514 [arXiv:2301.08274] [INSPIRE].

[85] T. Blum et al., *An update of Euclidean windows of the hadronic vacuum polarization*, arXiv:2301.08696 [INSPIRE].

[86] M. Hoferichter and T. Teubner, *Mixed Leptonic and Hadronic Corrections to the Anomalous Magnetic Moment of the Muon*, *Phys. Rev. Lett.* **128** (2022) 112002 [arXiv:2112.06929] [INSPIRE].

[87] CMD-3 collaboration, *Study of the process $e^+e^- \to 3(\pi^+\pi^-)\pi^0$ in the C.M. Energy range 1.6–2.0 GeV with the CMD-3 detector*, *Phys. Lett. B* **792** (2019) 419 [arXiv:1902.06449] [INSPIRE].

[88] X. Liu, Q.-S. Zhou and L.-M. Wang, *Broad resonance structure in $e^+e^- \to f_1(1285)\pi^+\pi^-$ and higher ρ-meson excitations*, *Phys. Rev. D* **106** (2022) 094012 [arXiv:2209.11525] [INSPIRE].

[89] W.A. Bardeen and W.K. Tung, *Invariant amplitudes for photon processes*, *Phys. Rev.* **173** (1968) 1423 [*Erratum ibid.* **4** (1971) 3229] [INSPIRE].

[90] R. Tarrach, *Invariant Amplitudes for Virtual Compton Scattering Off Polarized Nucleons Free from Kinematical Singularities, Zeros and Constraints*, *Nuovo Cim. A* **28** (1975) 409 [INSPIRE].

[91] WA76 and Athens-Bari-Birmingham-CERN-College de France collaborations, *Study of the $\eta\pi^+\pi^-$ system centrally produced in the reaction $pp \to p_f(\eta\pi^+\pi^-)p_s$ at 300 GeV/c*, *Z. Phys. C* **52** (1991) 389 [INSPIRE].

[92] WA102 collaboration, *A measurement of the branching fractions of the $f_1(1285)$ and $f_1(1420)$ produced in central pp interactions at 450 GeV/c*, *Phys. Lett. B* **440** (1998) 225 [hep-ex/9810003] [INSPIRE].

[93] T. Hahn, *CUBA: A library for multidimensional numerical integration*, *Comput. Phys. Commun.* **168** (2005) 78 [hep-ph/0404043] [INSPIRE].

[94] E.L. Lomon and S. Pacetti, *Time-like and space-like electromagnetic form factors of nucleons, a unified description*, *Phys. Rev. D* **85** (2012) 113004 [*Erratum ibid.* **86** (2012) 039901] [arXiv:1201.6126] [INSPIRE].

[95] B. Moussallam, *Unified dispersive approach to real and virtual photon-photon scattering at low energy*, *Eur. Phys. J. C* **73** (2013) 2539 [arXiv:1305.3143] [INSPIRE].

[96] A. Crivellin and M. Hoferichter, *Width effects of broad new resonances in loop observables and application to $(g-2)_\mu$*, *Phys. Rev. D* **108** (2023) 013005 [arXiv:2211.12516] [INSPIRE].

[97] COMPASS collaboration, *Resonance Production and $\pi\pi$ S-wave in $\pi^- + p \to \pi^-\pi^-\pi^+ + p_{recoil}$ at 190 GeV/c*, *Phys. Rev. D* **95** (2017) 032004 [arXiv:1509.00992] [INSPIRE].

JHEP08(2023)209

[98] F. von Hippel and C. Quigg, *Centrifugal-barrier effects in resonance partial decay widths, shapes, and production amplitudes*, Phys. Rev. D **5** (1972) 624 [INSPIRE].

[99] R. Mertig, M. Bohm and A. Denner, *FeynCalc: Computer algebraic calculation of Feynman amplitudes*, Comput. Phys. Commun. **64** (1991) 345 [INSPIRE].

[100] V. Shtabovenko, R. Mertig and F. Orellana, *New Developments in FeynCalc 9.0*, Comput. Phys. Commun. **207** (2016) 432 [arXiv:1601.01167] [INSPIRE].

[101] V. Shtabovenko, R. Mertig and F. Orellana, *FeynCalc 9.3: New features and improvements*, Comput. Phys. Commun. **256** (2020) 107478 [arXiv:2001.04407] [INSPIRE].

[102] A. Denner and S. Dittmaier, *Reduction of one loop tensor five point integrals*, Nucl. Phys. B **658** (2003) 175 [hep-ph/0212259] [INSPIRE].

[103] A. Denner and S. Dittmaier, *Reduction schemes for one-loop tensor integrals*, Nucl. Phys. B **734** (2006) 62 [hep-ph/0509141] [INSPIRE].

[104] A. Denner and S. Dittmaier, *Scalar one-loop 4-point integrals*, Nucl. Phys. B **844** (2011) 199 [arXiv:1005.2076] [INSPIRE].

[105] A. Denner, S. Dittmaier and L. Hofer, *Collier: a fortran-based Complex One-Loop LIbrary in Extended Regularizations*, Comput. Phys. Commun. **212** (2017) 220 [arXiv:1604.06792] [INSPIRE].

[106] H. Schäfer, M. Zanke, Y. Korte and B. Kubis, *The semileptonic decays $\eta^{(\prime)} \to \pi^0\ell^+\ell^-$ and $\eta' \to \eta\ell^+\ell^-$ in the standard model*, arXiv:2307.10357 [INSPIRE].

[107] M. Hoferichter, B.-L. Hoid, B. Kubis and J. Lüdtke, *Improved Standard-Model prediction for $\pi^0 \to e^+e^-$*, Phys. Rev. Lett. **128** (2022) 172004 [arXiv:2105.04563] [INSPIRE].

[108] M. Hoferichter, B. Kubis and M. Zanke, *Radiative resonance couplings in $\gamma\pi \to \pi\pi$*, Phys. Rev. D **96** (2017) 114016 [arXiv:1710.00824] [INSPIRE].

[109] M. Hoferichter, B. Kubis and D. Sakkas, *Extracting the chiral anomaly from $\gamma\pi \to \pi\pi$*, Phys. Rev. D **86** (2012) 116009 [arXiv:1210.6793] [INSPIRE].

[110] D.V. Amelin et al., *Study of the decay $f_1(1285) \to \rho^0(770)\gamma$*, Z. Phys. C **66** (1995) 71 [INSPIRE].

[111] S.I. Bityukov et al., *Observation of $D(1285) \to \phi\gamma$ Radiative Decay*, Phys. Lett. B **203** (1988) 327 [INSPIRE].

[112] Particle Data Group collaboration, *Review of Particle Physics*, PTEP **2022** (2022) 083C01 [INSPIRE].

[113] WA76 collaboration, *Study of the $\pi^+\pi^+\pi^-\pi^-$ System Centrally Produced by Incident π^+ and p Beams at 85 GeV/c*, Z. Phys. C **43** (1989) 55 [INSPIRE].

[114] WA76 collaboration, *Evidence for New States Produced in the Central Region in the Reaction $pp \to p_f(\pi^+\pi^-\pi^+\pi^-)p_s$ at 300 GeV/c*, Phys. Lett. B **228** (1989) 536 [INSPIRE].

[115] WA102 collaboration, *A study of the $K\bar{K}\pi$ channel produced centrally in pp interactions at 450 GeV/c*, Phys. Lett. B **413** (1997) 225 [hep-ex/9707022] [INSPIRE].

[116] Amsterdam-CERN-Nijmegen-Oxford collaboration, *Production and Decay Properties of the $D(1285)$ Meson in K^-p Interactions at 4.2 GeV/c*, Nucl. Phys. B **151** (1979) 181 [INSPIRE].

JHEP08(2023)209

[117] T. Bolton et al., *Observation of $f_1(1285) \to \pi^+\pi^-\pi^+\pi^-$ in radiative J/ψ decays*, Phys. Lett. B **278** (1992) 495 [INSPIRE].

[118] MARK-III collaboration, *Study of the Doubly Radiative Decay $J/\psi \to \gamma\gamma\rho^0$*, Phys. Rev. D **41** (1990) 1410 [INSPIRE].

[119] M.J. Corden et al., *Observation of the D, E and δ Mesons in $\pi^- p$ Interactions at 12 GeV/c and 15 GeV/c*, Nucl. Phys. B **144** (1978) 253 [INSPIRE].

[120] CLAS collaboration, *Photoproduction of the $f_1(1285)$ Meson*, Phys. Rev. C **93** (2016) 065202 [arXiv:1604.07425] [INSPIRE].

[121] J.H. Campbell et al., *Study of $D^0 \to \pi^\pm\delta^\mp$ and $\delta^\mp \to \pi^\mp\eta$ in the reaction $\pi^+ d \to p_s p D^0$ at 2.7 GeV/c*, Phys. Rev. Lett. **22** (1969) 1204 [INSPIRE].

[122] C. Defoix et al., *Evidence for decays of the D- and E-mesons into $\delta\pi$ in $\bar{p}p$ annihilation at 700 MeV/c*, Nucl. Phys. B **44** (1972) 125 [INSPIRE].

[123] WA76 collaboration, *Study of the $\pi^+\pi^-\gamma$ system centrally produced in the reaction $pp \to p_f(\pi^+\pi^-\gamma)p_s$ at 300 GeV/c*, Z. Phys. C **54** (1992) 371 [INSPIRE].

[124] BELLE collaboration, *High-Statistics Study of the $\tau^- \to \pi^-\pi^0\nu_\tau$ Decay*, Phys. Rev. D **78** (2008) 072006 [arXiv:0805.3773] [INSPIRE].

[125] BABAR collaboration, *Precise Measurement of the $e^+e^- \to \pi^+\pi^-(\gamma)$ Cross Section with the Initial-State Radiation Method at BABAR*, Phys. Rev. D **86** (2012) 032013 [arXiv:1205.2228] [INSPIRE].

[126] R. García-Martín, R. Kamiński, J.R. Peláez and J. Ruiz de Elvira, *Precise determination of the $f_0(600)$ and $f_0(980)$ pole parameters from a dispersive data analysis*, Phys. Rev. Lett. **107** (2011) 072001 [arXiv:1107.1635] [INSPIRE].

[127] JPAC collaboration, *Pole position of the $a_1(1260)$ from τ-decay*, Phys. Rev. D **98** (2018) 096021 [arXiv:1810.00016] [INSPIRE].

[128] P. d'Argent et al., *Amplitude Analyses of $D^0 \to \pi^+\pi^-\pi^+\pi^-$ and $D^0 \to K^+K^-\pi^+\pi^-$ Decays*, JHEP **05** (2017) 143 [arXiv:1703.08505] [INSPIRE].

[129] COMPASS collaboration, *Light isovector resonances in $\pi^- p \to \pi^-\pi^-\pi^+ p$ at 190 GeV/c*, Phys. Rev. D **98** (2018) 092003 [arXiv:1802.05913] [INSPIRE].

JHEP08(2023)209